THESIS

ASSESSING THE IMPACT OF STRATOSPHERIC AEROSOL INJECTION ON CONVECTIVE WEATHER ENVIRONMENTS IN THE UNITED STATES

Submitted by

Ivy Glade

Department of Atmospheric Science

In partial fulfillment of the requirements

For the Degree of Master of Science

Colorado State University

Fort Collins, Colorado

Summer 2023

Master's Committee:

Advisor: James W. Hurrell

Kristen L. Rasmussen
Brooke Anderson

ABSTRACT

ASSESSING THE IMPACT OF STRATOSPHERIC AEROSOL INJECTION ON CONVECTIVE WEATHER ENVIRONMENTS IN THE UNITED STATES

Continued climate warming, together with the overall development and implementation of climate mitigation and adaptation approaches, has prompted increasing research into the potential of proposed solar climate intervention (SCI) methods, such as stratospheric aerosol injection (SAI). SAI would reflect a small amount of incoming solar radiation away from the Earth to reduce warming due to increasing greenhouse gas concentrations. Research into the possible risks and benefits of SAI relative to the risks from climate change is emerging. There is not yet, however, an adequate understanding of how SAI might impact human and natural systems. To date, little or no research has been done to examine how SAI might impact environmental conditions critical to the formation of severe convective weather over the United States (U.S.), for instance. We use parallel ensembles of Earth system model simulations of future climate change, with and without hypothetical SAI deployment, to examine possible future changes in thermodynamic and kinematic parameters critical to the formation of severe weather during convectively active seasons over the U.S. Southeast and Midwest. We find that simulated forced changes in thermodynamic parameters are significantly reduced under SAI relative to a no-SAI world, while simulated changes in kinematic parameters are more difficult to distinguish. We also find that unforced internal climate variability may significantly modulate the projected forced climate changes over large regions of the U.S.

ACKNOWLEDGEMENTS

I would like to acknowledge my advisor, Dr. James W. Hurrell for his support in the completion of this work, as well as for the confidence he has always had in me to be a successful graduate student. I would also like to acknowledge Dr. Lantao Sun who calculated the convective weather environment parameters used in this research and who provided assistance in the computational challenges associated with the analysis of large datasets. Dr. Kristen L. Rasmussen, who provided expertise on mesoscale and related processes, served on my committee and has also included me in her research group activities, perhaps as an, ”honorary member,” has also been an instrumental part of my Master’s work. Finally, I would like to acknowledge Dr. Brooke Anderson for her role on my Master’s committee.

This work was supported by NOAA Grant #NA22OAR4320473. The GLENS and ARISE-SAI datasets were produced and maintained by the National Center for Atmospheric Research (NCAR) and are freely available on the NCAR Climate Data Gateway. The ARISE-SAI-UKESM1.0 dataset was produced and maintained by the U.K. Met Office. The University Cooperation for Atmospheric Research (UCAR) provided computational resources.

I am also grateful to my friends, family, and undergraduate mentors for the encouragement and support they have provided throughout both undergrad and my Master’s work. My parents have always been my biggest supporters in all that I do, and their continued belief in me has always given me more confidence in myself. In particular, I will forever be appreciative of my dad for showing me the importance of pursuing a career that I am passionate about. My undergraduate advisor, Dr. Phillip Larson, saw my passion for science and gave me opportunities to grow as a student and a researcher. Dr. Nicholas Metz, my REU advisor, gave me confidence in my ability to conduct scientific research and has continued to support me as I continue to progress in my academic career.

TABLE OF CONTENTS

CHAPTER 1: INTRODUCTION

Global carbon dioxide (CO_2) emissions have increased every decade since the 1960s, and they are projected to continue to increase over at least the next several decades (Friedlingstein et al., 2022; Jiang & Guan, 2016; Peters et al., 2012). It is therefore very unlikely that global climate warming will be limited to 1.5° or even 2°C above pre-industrial temperatures unless action is taken soon to drastically reduce emissions (IPCC, 2021). In fact, climate warming is projected to be over 2°C by the end of the century under moderate and current policy-relevant emissions scenarios, surpassing what is considered to be a safe threshold of warming (IPCC, 2021; Riahi et al., 2017; UNEP, 2022). Climate impacts such as drought intensification (Mukherjee et al., 2018; Strzepek et al., 2010), increases in extreme precipitation (Allen & Ingram, 2002; Donat et al., 2016) and continued sea ice loss (Stroeve et al., 2012; Wang & Overland, 2012) are projected to worsen over the coming decades (IPCC, 2021). Future changes also include the potential for increases in the frequency and intensity of severe convective weather over large portions of the United States (U.S.) (Diffenbaugh et al., 2013; Hoogewind et al., 2017; Lepore et al., 2021; Rasmussen et al., 2020; Seeley & Romps, 2015; Tippett et al., 2015; Trapp et al., 2007, 2009, 2019).

Given the urgency to limit continued temperature warming, the U.S. National Academies of Science, Engineering and Medicine (NASEM) recommended the formation of a transdisciplinary research program to identify the potential benefits and risks of solar climate intervention (SCI) relative to the risks posed by climate change (NASEM 2021). Most SCI approaches would cool the planet by reflecting a small amount of incoming solar radiation away from Earth, potentially minimizing some of the worst consequences of anthropogenic climate change while buying more time for mitigation and the deployment of CO_2 removal technologies. Stratospheric aerosol injection (SAI) is one proposed form of SCI that would involve, perhaps, the injection of sulfur

dioxide (SO2) into the stratosphere, which would react with hydrogen and oxygen to form highly reflective sulfate aerosols (Crutzen, 2006; Rasch et al., 2008; Richter et al., 2022).

Several Earth-system models have been used to simulate a future climate with SAI under different climate change scenarios (Kravitz et al., 2011; Kravitz et al., 2015; Richter et al., 2022; Tilmes et al., 2018; Visioni et al., 2023). Research to date has included examining changes in global and regional temperature and precipitation (Hueholt et al., 2023; Richter et al., 2022; Tilmes et al., 2018), atmospheric circulation patterns (Bednarz et al., 2022; Haywood et al., 2022), extreme temperature and precipitation events (Barnes et al., 2022; Ji et al., 2018), and ecological responses (Zarnetske et al., 2021), in addition to potential deployment technologies (Lockley et al., 2020; Smith & Wagner, 2018). Such studies have demonstrated that SAI could potentially be deployed to stabilize or reduce global mean temperature to a specific temperature target (Richter et al., 2022; Tilmes et al., 2018; Visioni et al., 2021); however, research that has been more regionally focused has indicated that regional impacts of SAI could be both positive and negative. For example, major African river basins may have enhanced drought risk because SAI is projected to cause precipitation decreases that overcompensate for projected increases due to climate warming (Abiodun et al., 2021). On the other hand, future projections indicate that SAI has the potential to reduce Greenland ice sheet mass loss (Moore et al., 2019) and minimize the loss of Arctic sea ice (Lee et al., 2023).

While research on the potential impacts of SAI has been increasing and broadening in recent years, current research remains scattered and ad hoc, so a holistic understanding of how SAI would impact Earth and human systems is limited (NASEM, 2021). For instance, while there have been studies documenting the impact of climate change on the large-scale environments in which severe weather (as defined by Galway, 1989) forms (Diffenbaugh et al., 2013; Franke et al., 2023; Hoogewind et al., 2017; Lepore et al., 2021; Rasmussen et al., 2020; Seeley & Romps, 2015; Trapp et al., 2007, 2009), we are not aware of any studies that have examined the potential impact of SAI on those environments. The topic is of relevance given the increasing costs of U.S. severe weather disasters in recent decades (NCEI 2022). Large-scale parameters and proxies have

been used to identify what environmental conditions are favorable to the formation of severe weather phenomena, largely in order to improve short-term predictability and overcome limitations in the limited observational record of severe weather (e.g., Doswell et al. 1996; Rasmussen & Blanchard 1998; Brooks et al. 2003; Craven & Brooks 2004). More recently, however, such parameters and proxies have been used to predict how the behavior of severe weather might change on longer time scales, such as through the end of the century (e.g., Diffenbaugh et al., 2013; Franke et al., 2023; Hoogewind et al., 2017; Lepore et al., 2021; Rasmussen et al., 2020; Trapp et al., 2007). In part, this is because running convection-permitting models over long periods of time is computationally expensive, and these parameters and proxies are resolvable using coarser resolution Earth-system models.

Parameters commonly analyzed include convective available potential energy (CAPE), convective inhibition (CIN), and the wind shear from the surface to $\sim$6 km (S06). With climate change, the magnitudes of both CAPE and CIN are projected to increase in the U.S. east of the Rocky Mountains in both the spring and summer (Diffenbaugh et al., 2013; Franke et al., 2023; Hoogewind et al., 2017; Lepore et al., 2021; Rasmussen et al., 2020; Trapp et al., 2007). Increases in the magnitude of CAPE and CIN have been attributed to increases in temperature and moisture throughout the troposphere (Rasmussen et al. 2020; see also Fig. 12). Wind shear (S06) is also generally projected to decrease in both the spring and summer seasons in the U.S., especially east of the Rockies (Trapp et al. 2007; Hoogewind et al. 2017; Lepore et al. 2021), a change that largely reflects decreases in the zonal wind at $\sim$6 km (Diffenbaugh et al., 2013; Franke et al., 2023).

Combined proxies that consider the integrated effects of more than one convective parameter have also been analyzed (Diffenbaugh et al., 2013; Hoogewind et al., 2017; Lepore et al., 2021; Seeley & Romps, 2015; Trapp et al., 2007, 2009). Proxies that consider both the thermodynamic and kinematic characteristics of the environments have been shown to better discriminate between environments conducive to ordinary thunderstorms, supercells, and tornadic supercells than individual thermodynamic or kinematic parameters alone (Rasmussen &

Blanchard, 1998). CAPES06, defined as the product of CAPE and S06, has been used to distinguish significant severe storms from those that are less severe (Brooks et al., 2003; Rasmussen & Blanchard, 1998). This proxy is often used in tandem with other convective weather parameters to describe whether an environment is favorable to the formation of severe weather on a given day (Diffenbaugh et al., 2013; Hoogewind et al., 2017; Lepore et al., 2021; Seeley & Romps, 2015; Trapp et al., 2007). The number of days with high magnitude CAPES06 are projected to increase with future warming across the eastern U.S. (Seeley & Romps, 2015). Diffenbaugh et al. (2013) suggests that CAPES06 is expected to increase across the eastern U.S. even though S06 is projected to decrease, because decreases in S06 are expected to occur on days when CAPE is already low.

Previous research examining projections of convective weather environments has mostly considered high emissions trajectories that are not consistent with current climate policies. In this study, we examine the potential impact of climate warming on convective weather environments in the U.S. using a 10-member ensemble of Earth-system model simulations under the Shared Socioeconomic Pathway 2-4.5 (SSP2-4.5) emissions scenario. This is a "middle of the road" scenario consistent with current climate policies that projects $\sim$2.7°C of global warming by the end of the century (O'Neill et al., 2017). It considers the slow development and deployment of sustainability practices such as CO_2 emissions reduction and removal technologies (IPCC, 2021; Riahi et al., 2017). In addition, we examine parallel climate change integrations with a hypothetical SAI deployment to examine the potential impact of SAI on large-scale convective weather environments, relative to the impacts from climate change alone. To our knowledge, this is the first study to examine the potential influence of SAI on future convective weather environments.

CHAPTER 2: METHODS

2.1 Model Information

This study utilizes a set of parallel simulations of climate change with and without SAI; specifically, the Assessing Responses and Impacts of Solar climate Intervention on the Earth system using stratospheric aerosol injection (ARISE-SAI; Richter et al., 2022). These simulations were performed using the freely available Community Earth System Model version 2 (CESM2), a fully coupled model with the Whole Atmosphere Community Climate Model version 6 (WACCM6) as the atmospheric component (Danabasoglu et al., 2020; Gettelman et al., 2019). WACCM6 is a high-top model with a well-represented stratosphere that includes 70 vertical levels with a model top of $4.5\text{x}10^{-6}$ hPa ($\sim$130 km) and a horizontal resolution of 1.25° longitude and 0.9° latitude (Danabasoglu et al., 2020). ARISE-SAI consists of two 10-member ensembles of climate change with and without SAI. Both ensembles follow the moderate SSP2-4.5 emissions scenario (O'Neill et al., 2017). The ARISE-SAI climate change simulations consist of five members that run from 2015-2100 and were carried out as a part of the Coupled Model Intercomparison Project Phase 6 (Eyring et al., 2016). Five other ensemble members cover the period from 2015-2069 and were branched off from three existing historical CESM2-WACCM6 simulations (1850-2014) with the addition of a small temperature perturbation at the first model time step (Richter et al., 2022).

The first five members of the ensemble with a hypothetical SAI deployment were initialized in 2035 using the first five members of the climate change (SSP2-4.5) ensemble. The last five members were initialized in a similar way, but with the addition of a small temperature perturbation (Richter et al., 2022). Each of the 10 SAI simulations extend through 2069, with SO2 being injected into the stratosphere continuously beginning in 2035 in order to maintain global mean temperature at $\sim$1.5°C above its pre-industrial value. In addition, the ARISE-SAI injection strategy is designed to maintain the equator-to-pole and interhemispheric temperature

gradients to values consistent with those observed at the 1.5°C temperature target (Kravitz et al., 2017; MacMartin et al., 2014; Richter et al., 2022). The stabilizing influence of SAI is clear when examining not only the time series of global 2 m temperature change (Hueholt et al., 2023; Richter et al., 2022), but also that for the contiguous U.S (CONUS) (Figure 1).

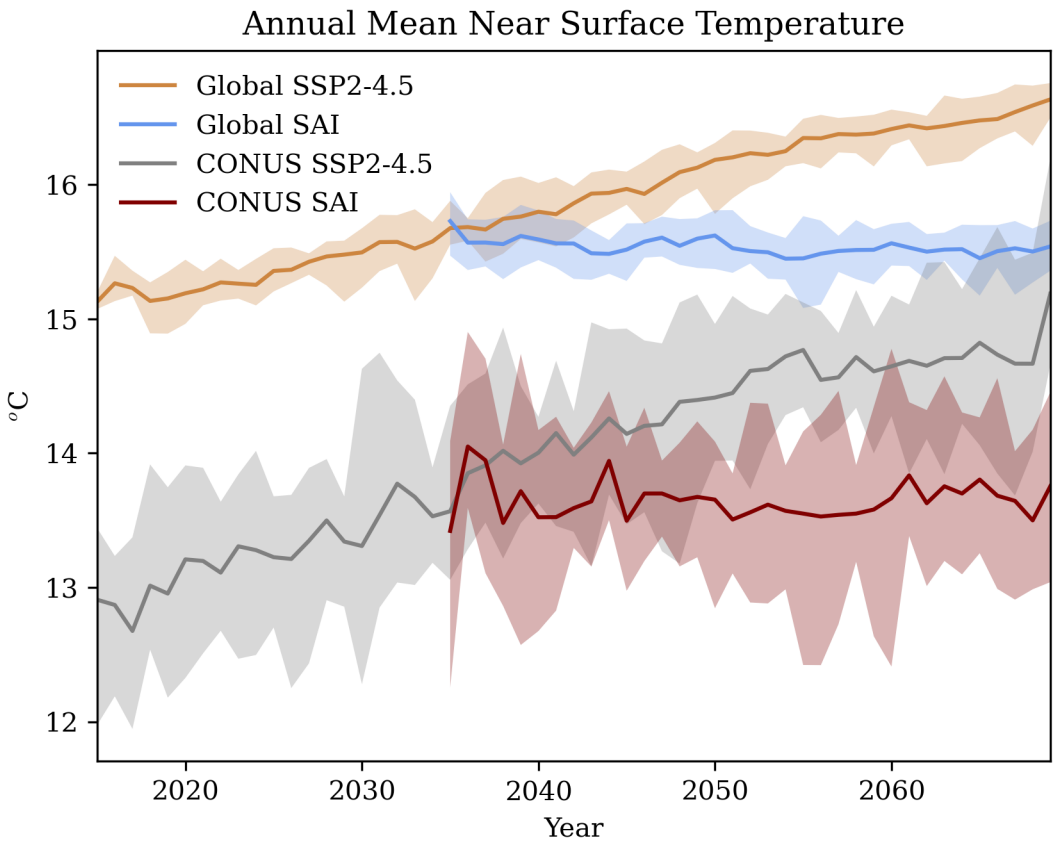

Figure 1 : Annual mean near-surface (2 m) temperature from the SSP2-4.5 simulations (2015-2069) and the simulations where SAI is deployed (2035-2069). Results averaged over the globe are given by the tan (SSP2-4.5) and blue (SAI) lines, while those averaged over the contiguous U.S. are given by the gray (SSP2-4.5) and red (SAI) lines. Ensemble means are shown by the thick solid lines, while the minimum and maximum ranges of the individual ensemble members are shown by the corresponding color shading.

2.2 Convective Weather Environment Parameters and Proxies

CAPE (J kg^{-1}) and CIN (J kg^{-1}) are thermodynamic parameters which consider the temperature and moisture content of the atmosphere (Doswell & Rasmussen, 1994). CAPE is a

measure of potential energy that is defined by the vertical integral of buoyancy from the level of free convection to the equilibrium level, and is analogous to updraft velocity (Doswell & Rasmussen, 1994; Rasmussen & Blanchard, 1998; Trapp et al., 2007). CIN represents the negative buoyancy and is indicative of the potential to suppress convective motions (Rasmussen & Blanchard, 1998). CAPE and CIN were calculated as the most-unstable parcel in the lowest 3000 m of the atmosphere, which is a useful method for capturing cases of elevated instability, while being effective at identifying low-level or surface-based instability when present (Doswell & Rasmussen, 1994).

S06 (m s^{-1}) is a kinematic parameter which is representative of the change in the horizontal wind vector from $\sim$10 m above ground-level to approximately 6 km altitude. This measure of wind shear is used to diagnose whether or not an environment is favorable to the formation of significant severe thunderstorms (Brooks et al., 2003; Rasmussen & Blanchard, 1998). In particular, small magnitudes of S06 are typically associated with the development of relatively small, short-lived single-cell thunderstorms, while larger magnitudes of S06 are typically associated with the potential for development of supercell thunderstorms, which are longer-lived, more organized, and more intense (Weisman & Klemp, 1982).

CAPES06 (m^3 s^{-3}) is a good discriminator for significant severe thunderstorm events (Brooks et al., 2003; Marsh et al., 2007; Rasmussen & Blanchard, 1998; Trapp et al., 2007). We consider CAPES06 as simply the product of CAPE and S06. Some previous studies have weighted S06 more heavily than CAPE (Brooks et al., 2003; Seeley & Romps, 2015), but Seeley & Romps (2015) note that varying the weight of S06 in calculations of CAPES06 did not have a large impact on future projections of favorable convective weather environments. Additionally, CAPES06 has not been frequently looked at as a standalone quantity. It is typically used with other parameters such as CAPE and S06 to identify convective weather environment days (Diffenbaugh et al., 2013; Hoogewind et al., 2017; Lepore et al., 2021; Seeley & Romps, 2015; Trapp et al., 2007). We elect to examine CAPES06 in this way since we are using daily mean

rather than sub-daily temporal resolution (see further discussion below), rendering commonly used minimum thresholds inappropriate for use.

While we present results as spatial maps over the CONUS, we also compute area-averaged statistics over the Southeast and Midwest regions. Analysis of area averaged quantities is beneficial since it allows for an additional analysis of the time evolution of the quantities considered with and without SAI. The Southeast is defined as the grid points bounded by 39°-48°N and 255°-274°W, while the Midwest is defined as the region within 30°-39°N and 255°-280°W (Figure 2). While we examined all seasons and other regions over the U.S., we restrict our analysis here to the Southeast region during the boreal spring season (MAM) and the Midwest region during the boreal summer season (JJA). These regions and seasons were chosen subjectively based on the climatological seasonal distributions of both convective weather environments and severe weather events (e.g., Kelly et al., 1985; Doswell et al., 2005; Brooks et al., 2007; Taszarek et al., 2020). The representation of convective weather environments in both the Community Atmosphere Model version 6 (CAM6) (Danabasoglu et al., 2020), an atmosphere only model, and CESM2-CAM6, a fully coupled Earth-system model, have been validated against the fifth generation of the high resolution global reanalysis dataset produced by ECMWF (ERA5) (Franke et al., 2023; Li et al., 2020). CAM6 is the low-top version of WACCM6, where the two models have the same vertical structure up to 87 hPa and nearly identical parameterizations (Danabasoglu et al., 2020). These validations have shown that both CAM6 and CESM2-CAM6 are able to well represent convective weather environments over the eastern CONUS, as well as the synoptic features (Li et al., 2020) and the influence of large-scale modes of variability, such as the El Niño Southern Oscillation (ENSO; Franke et al., 2023).

Most previous studies that have considered convective weather environment parameters have calculated these indices using model output at 00 Z, which is known to represent the time when CAPE is maximized (e.g., Trapp et al., 2007; Diffenbaugh et al., 2013; Seeley & Romps, 2015). However, only daily mean data are available for all 10 of the ARISE-SAI ensemble members. To assess the suitability of using daily averaged data, we extracted data at 00 Z from

one ensemble member from the CESM2 Large Ensemble (CESM2-LE) (Rodgers et al., 2021) and compared results to those computed from daily average data. The CESM2-LE is a 100-member ensemble that runs from 1850-2100 and follows the SSP3-7.0 emissions scenario, which warms more and has slower development of mitigation and adaptation practices relative to SSP2-4.5 (O'Neill et al., 2017). The CESM2-LE utilizes the low-top atmospheric component of CESM2 (CAM6; Rodgers et al., 2021).

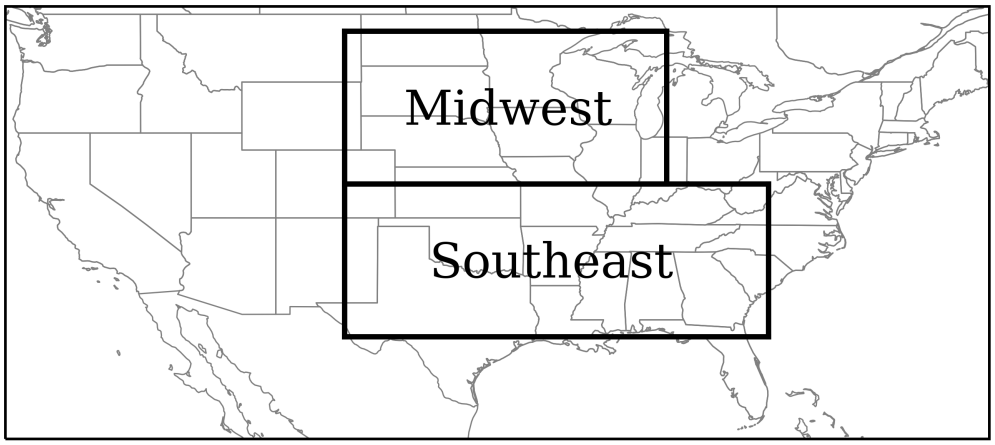

Figure 2 : The Midwest and Southeast regions. The Midwest is defined by the grid points bounded by 30°-39°N and 255°-280°W. The Southeast is defined by the grid points bounded by 39°-48°N and 255°-274°W.

We compared the time evolutions of CAPE, CIN, S06, and CAPES06 computed at 00 Z to those computed as a daily mean quantity from 2015-2069. The analysis was based on anomalies relative to 1971-2000 climatologies. The time evolution of CAPES06 anomalies for the Southeast in MAM and the Midwest in JJA indicates high correlation between the sub-daily and daily mean anomalies in both regions ($r = 0.988$ and $r = 0.946$) (Figure 3). Correlations between sub-daily and daily mean anomalies are similarly high for CAPE, CIN and S06 (not shown). Thus, while differences exist in the absolute magnitude of the convective parameters when computed from sub-daily relatively to daily mean data (especially for CIN, which is maximized at night rather than in the afternoon), the changes over time of the parameters computed from daily mean data, as well as the differences between the SAI and no-SAI simulations, are very similar to the

temporal changes of the parameters computed from 00 Z data only. Using the daily mean data that is available from all 10 ARISE-SAI ensemble members allows us to better estimate forced changes in climate, as well as better examine how the forced changes might be modified by decadal and multi-decadal internal climate variability.

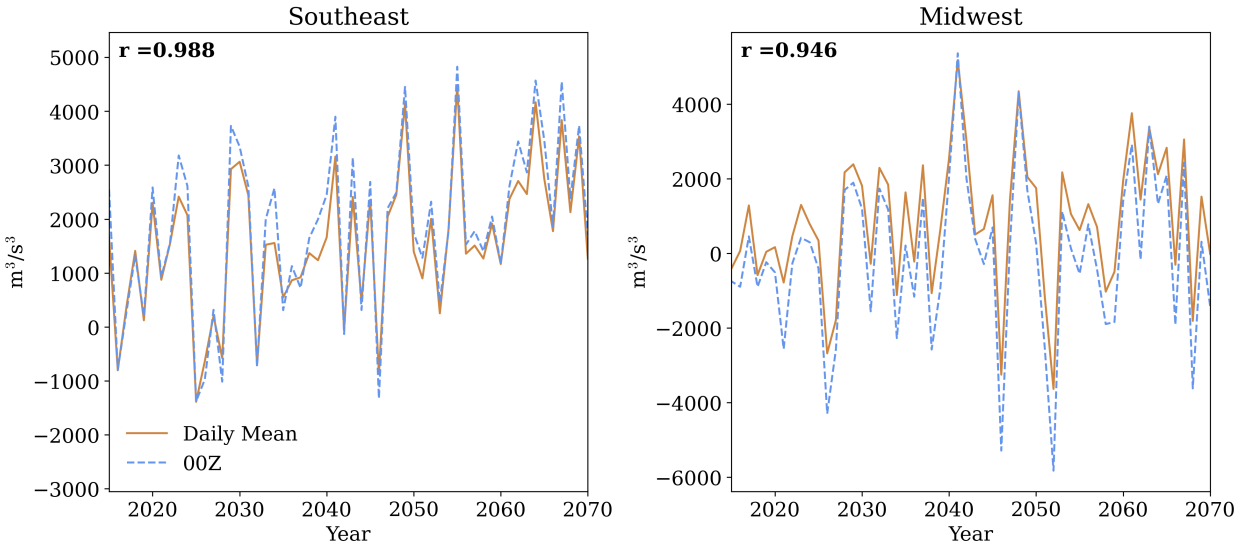

Figure 3 : Time series of CAPES06 anomalies in the Southeast in MAM and in the Midwest in JJA from 2015-2070 from one member of the CESM2 Large Ensemble. Anomalies are relative to the 2015-2034 mean. The tan line represents CAPES06 anomalies calculated from daily mean data, while the blue dashed line represents CAPES06 anomalies from 00 Z data only. The correlation between the two time series is the r-value in the top left of each graph.

CHAPTER 3: RESULTS

3.1 Forced Responses

Differences in future projections with and without SAI are evident in many convective weather environment parameters averaged over the Southeast and Midwest regions (Figure 4). Without SAI deployment, CAPE increases throughout the time period relative to the base period (2015-2034), but with SAI deployment CAPE stabilizes (Figure 4a, 4e). Similarly, climate change causes an increase in the magnitude of CIN (increasingly negative values) in both regions while SAI stabilizes CIN near 2035 levels in these simulations (Figure 4b, 4f). S06 decreases in magnitude throughout the time period in the no-SAI simulations, but the influence of SAI on wind shear is less clear (Figure 4c, 4g). The sign of future greenhouse-gas induced changes in CAPE, CIN and S06 are in general agreement with previous studies (Diffenbaugh et al., 2013; Lepore et al., 2021; Trapp et al., 2009), although magnitudes differ, at least in part, because earlier studies examined climate change scenarios other than SSP2-4.5. Projected increases in the magnitude of CAPES06, which are dominated by increases in CAPE with continued climate warming (Figure 4d, 4h,) are also in line with earlier studies (Diffenbaugh et al., 2013; Seeley & Romps, 2015; Trapp et al., 2007). It thus follows that changes in CAPES06 mirror the simulated changes to CAPE in the SAI runs, with anomalies stabilizing to approximately 2035 levels (Figure 4d, 4h).

The underlying climatological (2015-2034) distributions of these parameters from the ARISE-SAI simulations (Figure 5) provide context for projected changes with and without SAI, and they are in good agreement with observations (e.g., Franke et al., 2023; Li et al., 2020). In MAM, maximum values of CAPE are found over the south-central U.S., especially just west of the Gulf of Mexico (Figure 5a). The area of maximum CAPE becomes much larger in JJA, with large values generally east of the Rockies and the greatest magnitudes over the far southern U.S. (Figure 5e). The changes between MAM and JJA are especially notable over the Northern Plains

and the Midwest, where CAPE in the summer has magnitudes near those of the Southeast in MAM (Figure 5e).

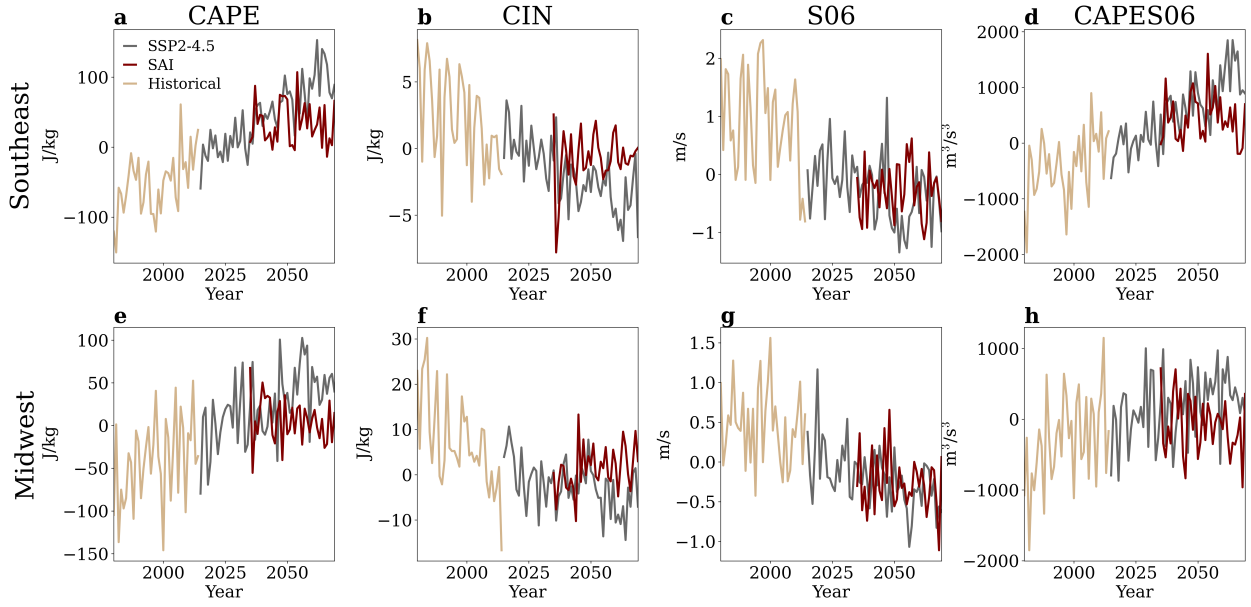

Figure 4 : Time series showing CAPE (J kg^{-1}) (a and e), CIN (J kg^{-1}) (b and f), S06 (m s^{-1}) (c and g), and CAPES06 (m^3 s^{-3}) (d and h) anomalies relative to the 2015-2034 mean for the Southeast in MAM (top row) and the Midwest in JJA (bottom row) from 1980-2069. The tan line represents the three-member ensemble mean from CESM2(WACCM6) historical runs, the gray line represents the 10-member ensemble mean from the SSP2-4.5 simulations, and the red line represents the 10-member ensemble mean from the simulations with SAI deployment beginning in 2035.

As for CAPE, the magnitude of CIN increases greatly from MAM to JJA (Figure 5b, 5f), although we again note the magnitudes of the climatological values from daily mean data are larger than in previous studies that have utilized data from the afternoon only. In particular, the largest magnitudes of CIN are concentrated over Texas, Oklahoma and Kansas in MAM, but by JJA the largest magnitudes are shifted to the central Great Plains. The deep-layer shear (S06) is positive over the entire U.S. during both seasons, although it is larger in spring than summer (Figure 5c, 5g). In both seasons, maximum values of shear are over the northern third of the U.S. The distribution of CAPES06 largely mirrors the distribution of CAPE in both MAM and JJA (Figure 5d, 5h), although CAPES06 has a more uniform distribution across the eastern half of the U.S. in JJA compared to CAPE (5d, 5h).

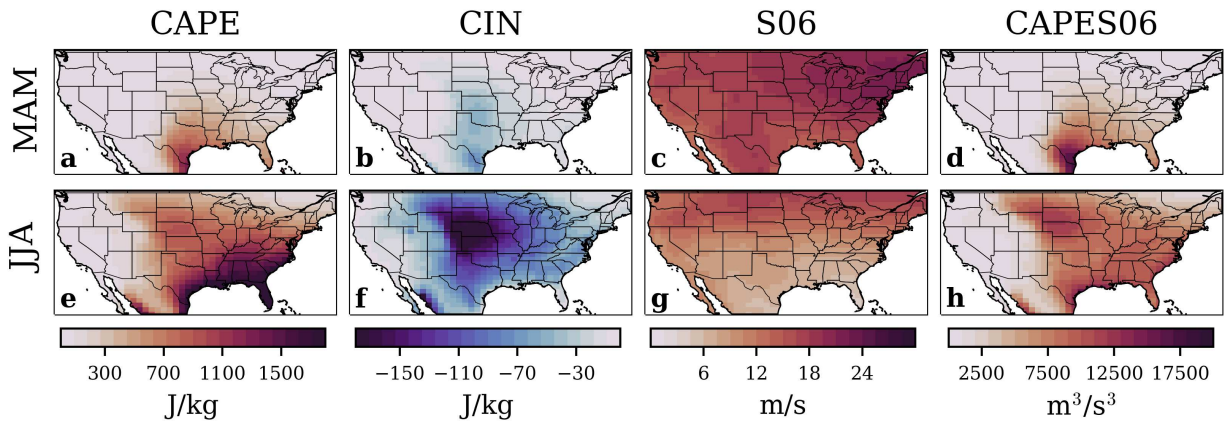

Figure 5 : Climatological CAPE (a and e), CIN (b and f), S06 (c and g) and CAPES06 (d and h) for MAM (top row) and JJA (bottom row) over 2015-2034 for the SSP2-4.5 simulations.

To examine how climate change affects these environmental parameters, we examine the average changes in the last decade of the ARISE-SAI simulations (2060-2069) relative to the climatological period (2015-2034; Figure 6). In the spring and summer, CAPE, CIN, and CAPES06 are all projected to increase in magnitude with climate change (Figure 6). Over most regions, these increases are statistically significant at the α=0.05 level for the two-sample t-test (to account for issues related to multiple testing across the U.S. domain, the method outlined in Wilks (2016) was used to control the false discovery rate). Wind shear (S06) is projected to decrease in magnitude during MAM across much of the U.S., with decreases largest in the eastern U.S. (Figure 6c). S06 is also projected to decrease in the summer months, with the largest decreases in the northwest U.S. where convective activity is not as significant historically (Figure 6g). While decreases in wind shear are evident across much of the U.S., the magnitude of the decrease is relatively small compared to the magnitude of the underlying climatology (Figure 5c, 5g, 6c, 6g): climatological S06 values exceed 20 m s^{-1} across much of the U.S., while projected changes by 2060-2069 exceed 1 m s^{-1} over only limited regions (Figure 6c, 6g). Projected increases in CAPE, CIN and CAPES06, as well as projected decreases in S06, are broadly consistent with previous literature (Diffenbaugh et al., 2013; Franke et al., 2023; Hoogewind et al., 2017; Lepore et al., 2021; Rasmussen et al., 2020; Seeley & Romps, 2015; Trapp et al., 2007, 2009).

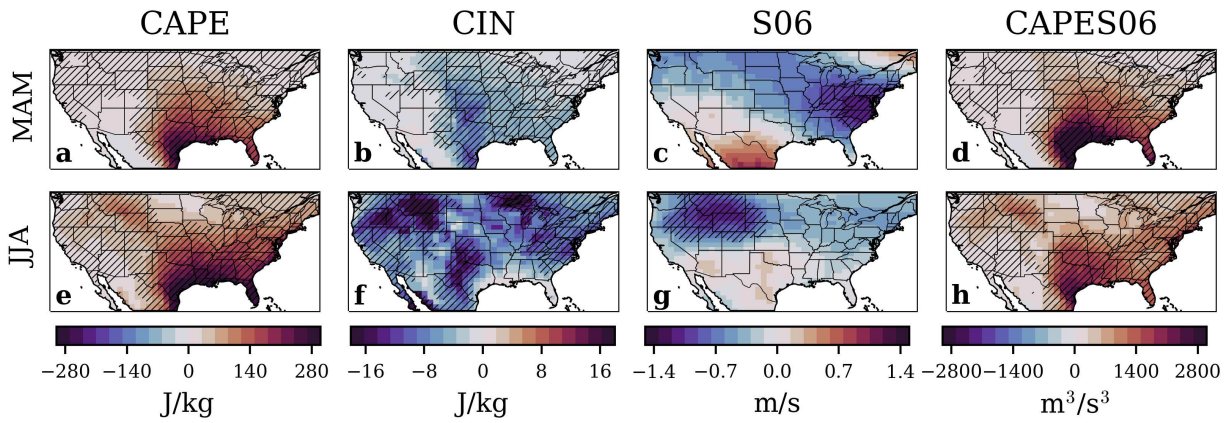

Figure 6 : The differences between 2060-2069 (SSP2-4.5) and 2015-2034 (SSP2-4.5) ensemble mean CAPE, CIN, S06, and CAPES06, in MAM (top row) and JJA (bottom row). Stippling indicates statistical significance at the α=0.05 level.

In the SAI simulations, future changes in the magnitudes in CAPE, CIN and CAPES06 are generally much smaller and less statistically significant across the U.S. (Figure 7) than in the no-SAI simulations (Figure 6). This suggests that if SAI were to be deployed, the convective weather environment parameters analyzed here would not change appreciably from today, although that conclusion may be specific to the ARISE-SAI simulations. Future changes in S06 with SAI, however, are generally similar to those projected in the no-SAI simulations. For instance, the spatial patterns of projected decreases in S06 with SAI are similar to those without SAI in MAM (Figure 6c, 7c), although regions of maximum decrease differ. Since an objective of the ARISE-SAI experiment is to not only keep global average temperature near its 2035 value but also to preserve the equator-to-pole temperature gradient (Richter et al., 2022), it is difficult to attribute the S06 decreases in the no-SAI simulations (Figure 6c) to changes in the thermal wind balance, as has been done previously (Trapp et al., 2007; Seeley & Romps, 2015). This suggests that there could be a different mechanism driving future changes in S06. We explore this aspect further in the Discussion. Another way to examine the impacts of SAI on convective weather parameters relative to the effects from increasing greenhouse concentrations alone is to directly difference the SAI and no-SAI simulations. Here we do so for differences averaged over the 2060-2069 decade. For CAPE, CIN, and CAPES06, the differences follow a similar spatial

pattern and magnitude, but are of opposite sign, to the projected future changes in the no-SAI simulations (Figure 6 and 8). Further, the differences between the SAI and no-SAI simulations for CAPE, CIN and CAPES06 are widely statistically significant across the eastern U.S. for 2060-2069, while the differences for S06 are not (Figure 8).

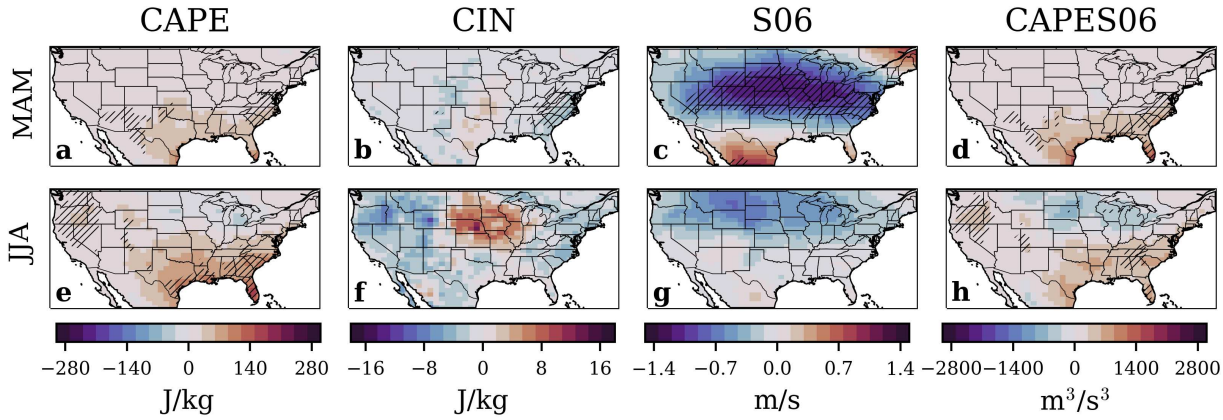

Figure 7 : Differences between 2060-2069 (SAI) and 2015-2034 (SSP2-4.5) ensemble mean CAPE, CIN, S06, and CAPES06, in MAM (top row) and JJA (bottom row). Stippling indicates statistical significance at the α=0.05 level.

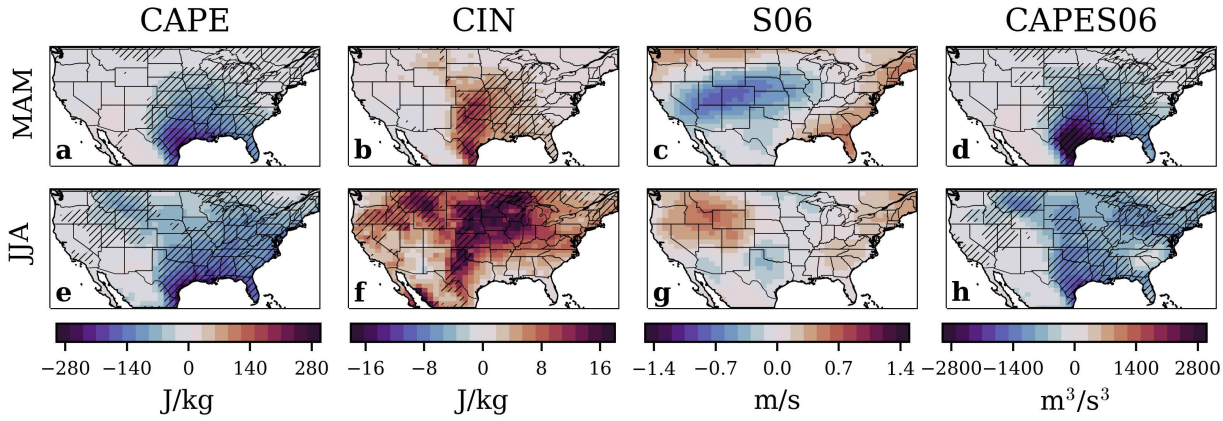

Figure 8 : Differences between SAI and SSP2-4.5 ensemble means for 2060-2069 in MAM (top row) and JJA (bottom row). Stippling indicates statistical significance at the α=0.05 level.

In addition to examining changes in each convective environment parameter separately, understanding their co-variability can provide insight into the potential change in the distributions of convective modes and frequency with and without SAI (Diffenbaugh et al., 2013; Lepore et al.,

2021; Rasmussen et al., 2020). To this point, bivariate distributions of convective parameters from 2060-2069 were created from daily data for the SAI and no-SAI simulations, respectively. For each individual ensemble member, daily mean values of CAPE, CIN and S06 were collected for each gridpoint over the Southeast in MAM and the Midwest in JJA. Distinct bivariate distributions (CAPE versus CIN, and CAPE versus S06) were then plotted for the difference of the SAI and no-SAI simulations (Figure 9 and 10). Positive numbers indicate that the SAI simulations had more days in a given bin than the no-SAI simulations, whereas negative numbers indicate the opposite.

In the Southeast in MAM and the Midwest in JJA, there are more days with low magnitudes of CAPE and CIN in the SAI simulations than in the no-SAI simulations, indicating that projected increases in the number of days with increased CAPE and CIN under SSP2-4.5 could be largely avoided with SAI (Figure 9). The shift in the distribution of these parameters is due to decreases in both CAPE and CIN, which is evident in the straight diagonal region that separates the red and blue points. The difference in the shape of the distributions between the Southeast in MAM (Figure 9a) and the Midwest in JJA (Figure 9b) is largely due to the climatology of CIN, where values have much higher magnitudes in the Midwest in JJA (Figure 5b, 5f).

The difference between the SAI and no-SAI simulations for the daily bivariate distribution of CAPE and S06 is illustrated in Figure 10. While the simulations suggest fewer days with high CAPE if SAI were to be deployed, the number of days with high shear is comparable between the SAI and no-SAI simulations. Thus, with SAI, there may be fewer days with high magnitude CAPE and S06, but the number of days with low-moderate CAPE and high shear may be similar with and without SAI (Figure 10).

The analyses in Figures 9 and 10 also begin to highlight the potential role of unforced, internal climate variability in projected future changes in convective weather environments with and without SAI. The potential for internal variability to significantly modulate projected forced changes in climate is known to be significant (e.g. Deser et al., 2012; Deser, 2020; Schwarzwald & Lenssen, 2022). In the next section, we are motivated by these and similar studies to go beyond

descriptions of only forced changes in climate warming in order to more completely examine the range of plausible future convective weather environments with and without SAI.

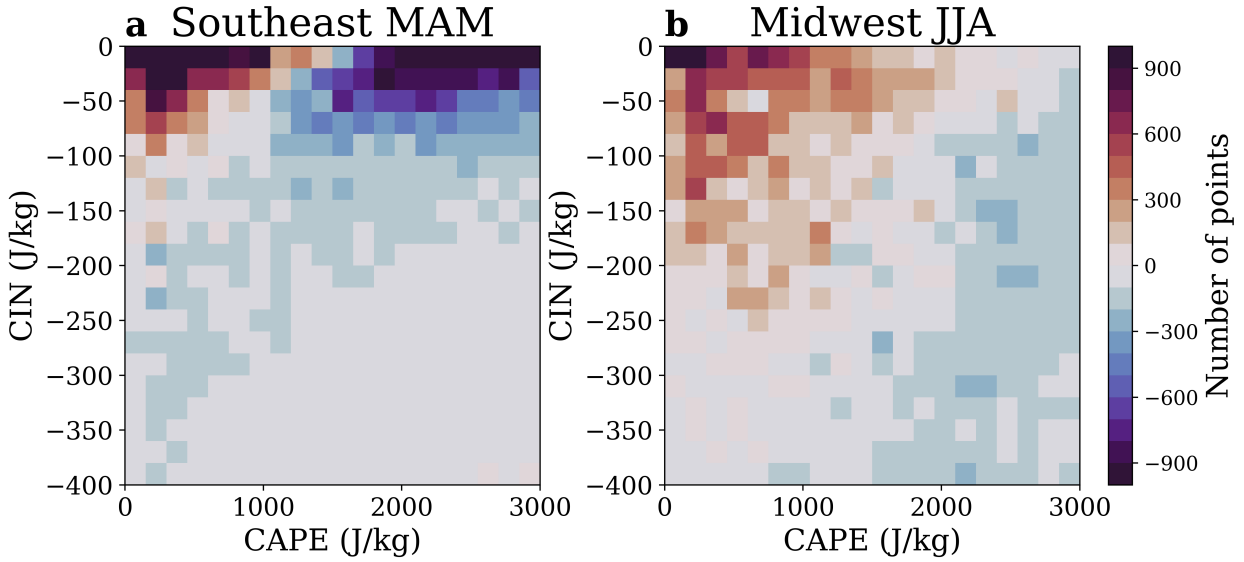

Figure 9 : The difference between the SAI and no-SAI simulations (i.e. SAI - SSP2-4.5) for the bivariate distribution of CAPE (x-axis) and CIN (y-axis) for the Southeast in MAM (a) and the Midwest in JJA (b) over 2060-2069. Red (blue) pixels represent bins where there are more (less) days with corresponding CAPE and CIN values in the simulations with SAI.

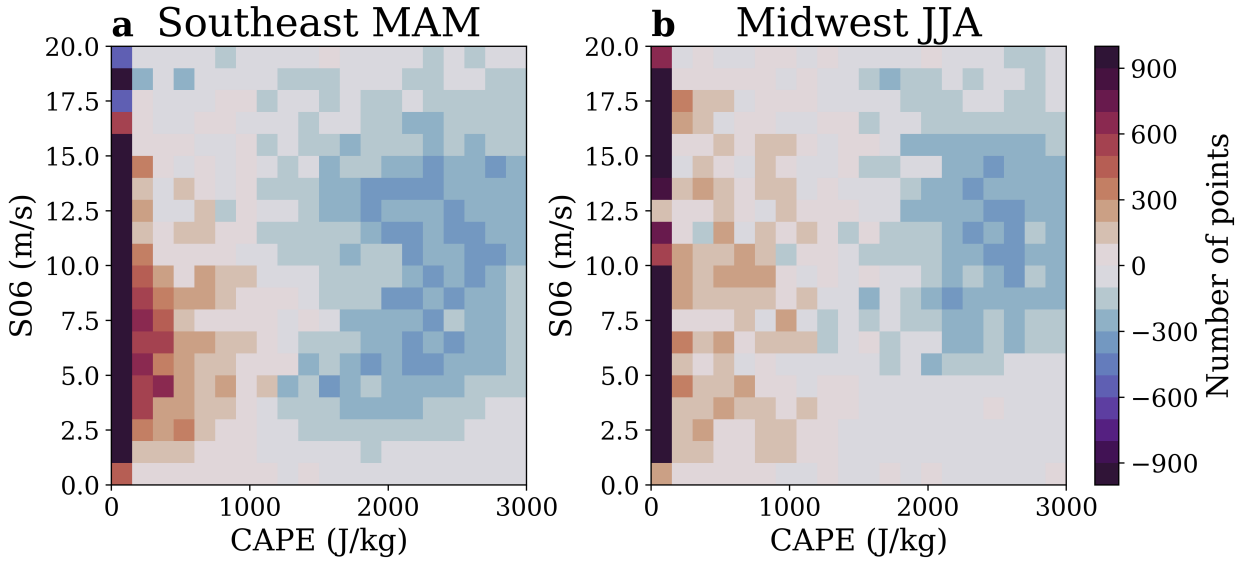

Figure 10 : As for Figure 9, but the difference between the SAI and no-SAI simulations (i.e. SAI - SSP2-4.5) for the bivariate distribution of CAPE (x-axis) and S06 (y-axis).

3.2 The Role of Internal Climate Variability

Other studies have examined the impact of internal climate variability on the behavior of severe weather related phenomena. However, they have tended to focus on sub-seasonal-to-interannual variations, such as those associated with the Madden Julian Oscillation (Baggett et al., 2018; Thompson & Roundy, 2013) or the El Niño Southern Oscillation (ENSO) phenomenon. For instance, Allen et al., (2018) examined the role of ENSO in modulating the annual cycle of tornadoes over the U.S., while Tippett et al., (2022) studied how ENSO and the phase of the Arctic Oscillation (AO) impacted the predictability of the tornado environment index. What has not been often considered, however, is the potential role that lower frequency (e.g., decadal) internal climate variability could play in future projections of severe weather. Ensemble simulations from climate and Earth system models indicate that even though the forced response to increasing greenhouse gas concentrations shows warming across the U.S. and other land regions, decadal and longer-timescale internal climate variability has the potential to significantly enhance or dampen the forced response (Deser et al., 2012; Hawkins & Sutton, 2009; Kay et al., 2015). It is thus relevant to consider how internal climate variability may impact future projections of convective weather environments both with and without SAI.

Histograms of changes in CAPE and CAPES06 by 2060-2069 relative to the reference period (2015-2034) show that while the forced response (ensemble mean) increases in magnitude under SSP2-4.5, changes in individual no-SAI simulations could be notably smaller or larger due to unforced variations in climate (Figure 11; gray bars). Specifically, individual ensemble members project changes in CAPE that depart as much as 60 J kg^{-1} from the ensemble mean increase of 107 J kg^{-1} by 2060-2029 (Figure 11a). Similar results are evident for CAPES06. For instance, while the ensemble-mean projected change in CAPES06 is an increase of 392 m^3 s^{-3} across the Midwest in JJA, one member projects a decrease of 226 m^3 s^{-3} by mid-century (Figure 11h). Such results confirm the large role that internal climate variability will play in the future evolution of climate, a point also emphasized recently by Franke et al. (2023) who examined

future decadal trends in convective environment variables using the CESM2 Large Ensemble under SSP3-7.0 (Rodgers et al., 2021).

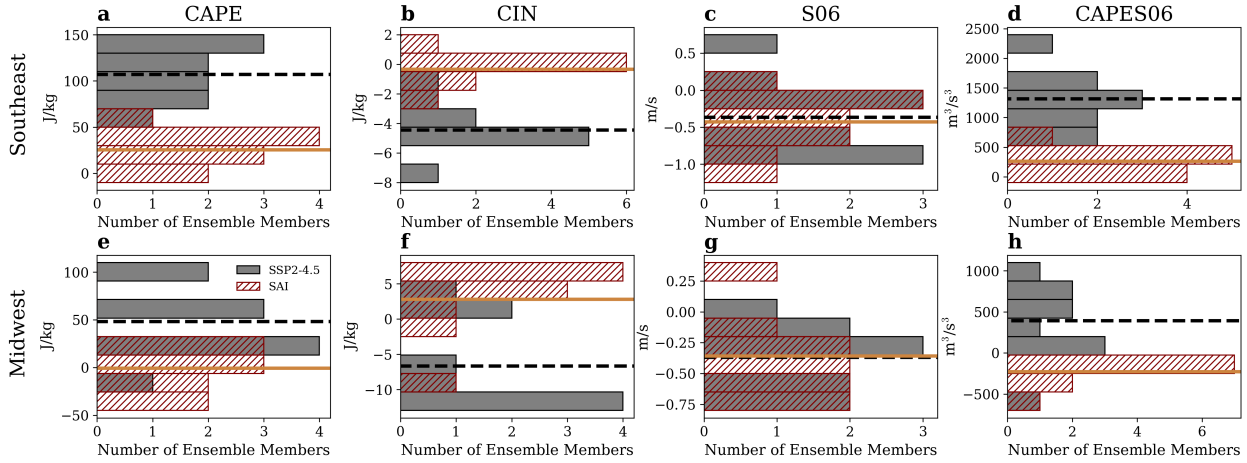

Figure 11 : Histograms of the 10 ensemble members of the SSP2-4.5 (gray bars) and SAI (red hatched bars) simulations, illustrating the change in CAPE, CIN, S06, and CAPES06 for 2060-2069 relative to the 2015-2034. The black dotted and solid tan lines represent the ensemble mean values of the SSP2-4.5 and SAI simulations, respectively. Results are for the Southeast in MAM (a-d) and the Midwest in JJA (f-h).

A similarly wide range of possible changes in CAPE, CIN and CAPES06 are evident in the SAI simulations as well (Figure 11; red hatched bars). Thus, while the forced signals in the convective parameters examined here are distinct in future worlds with and without SAI, internal climate variability could produce similar climate outcomes in the decades ahead (Keys et al., 2022). For example, an ensemble member in the no-SAI simulation projects that CIN decreases in magnitude by 5.2 J kg^{-1} in JJA by 2060-2069, while a member in the SAI simulation projects an 8.5 J kg^{-1} increase in CIN over the same period (Figure 11f). Additionally, the distribution of possible future changes in S06 with and without SAI are very similar across ARISE-SAI ensemble members when averaged over the Southeast and Midwest regions, as is the case for the ensemble-mean changes (Figure 11c, 11g). This further supports the idea that the thermal wind relationship may not be the primary mechanism governing future changes in the deep-layer tropospheric wind shear over the U.S.

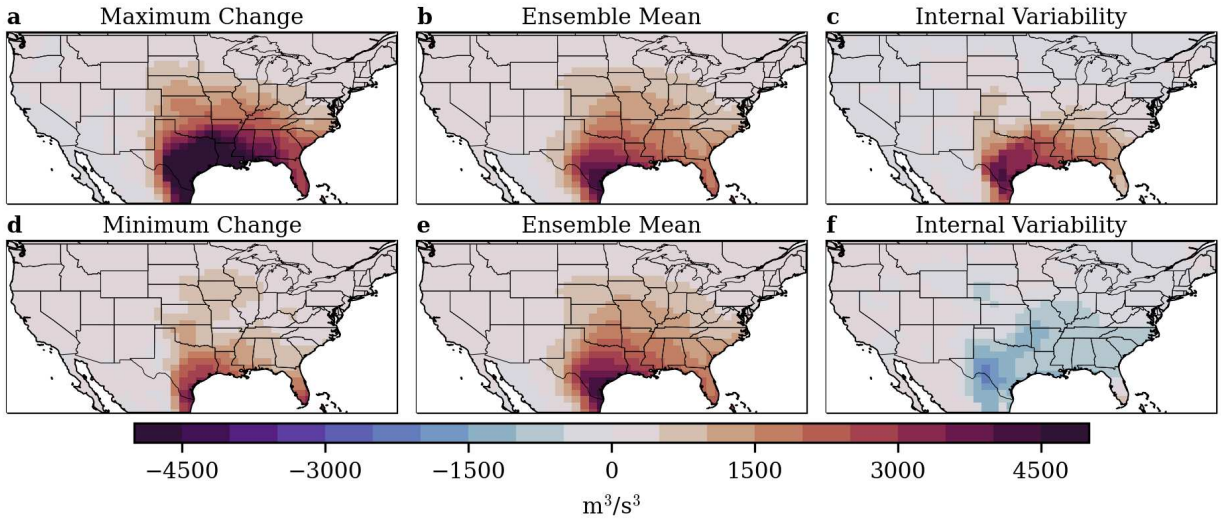

Figure 12 : The ensemble members with the maximum (a) and minimum (b) changes in CAPES06 by 2060-2069 relative to 2015-2034 over the Southeast in MAM in the SSP2-4.5 simulations, calculation described in text. The forced response, or ensemble mean, is shown in (b) and repeated in (e). The change in CAPES06 due only to internal variability is shown for the ensemble member with the maximum and minimum change in (c) and (f), respectively.

To further illustrate the extent to which internal climate variability can produce a climate outcome that differs significantly from the forced response alone, we subjectively chose the ensemble member with the maximum change in CAPES06 by 2060-2069 when averaged over the Southeast in MAM, and contrasted it against the ensemble member with the smallest change. The spatial patterns of change for each of these two ensemble members is shown, along with the ensemble mean changes (Figure 12). By subtracting the ensemble mean changes from the total changes in CAPES06, the regional changes due only to internal climate variability are revealed. The main point is that internal climate variability may either significantly enhance the forced response due to climate change (Figure 12c) or suppress it (Figure 12f) on decadal time scales. It is also notable that the magnitudes of the changes due solely to internal climate variability are spatially coherent over large regions, and they are of similar magnitude to the force changes (e.g., Deser, 2020).

CHAPTER 4: DISCUSSION

In ARISE-SAI, projected future changes in CAPE, CIN, and CAPES06 are smaller with simulated SAI deployment than what is projected with climate change alone (Figure 6, 7). This is consistent with lower temperatures and dew points on average throughout the troposphere in MAM and JJA in an SAI future (Figure 13). It thus follows that the SAI simulations have fewer co-occurrences of high magnitude CAPE and CIN in the future (Figure 9), whereas changes in the bivariate distribution of CAPE and S06 are primarily driven by smaller values of CAPE in a future with SAI (Figure 10).

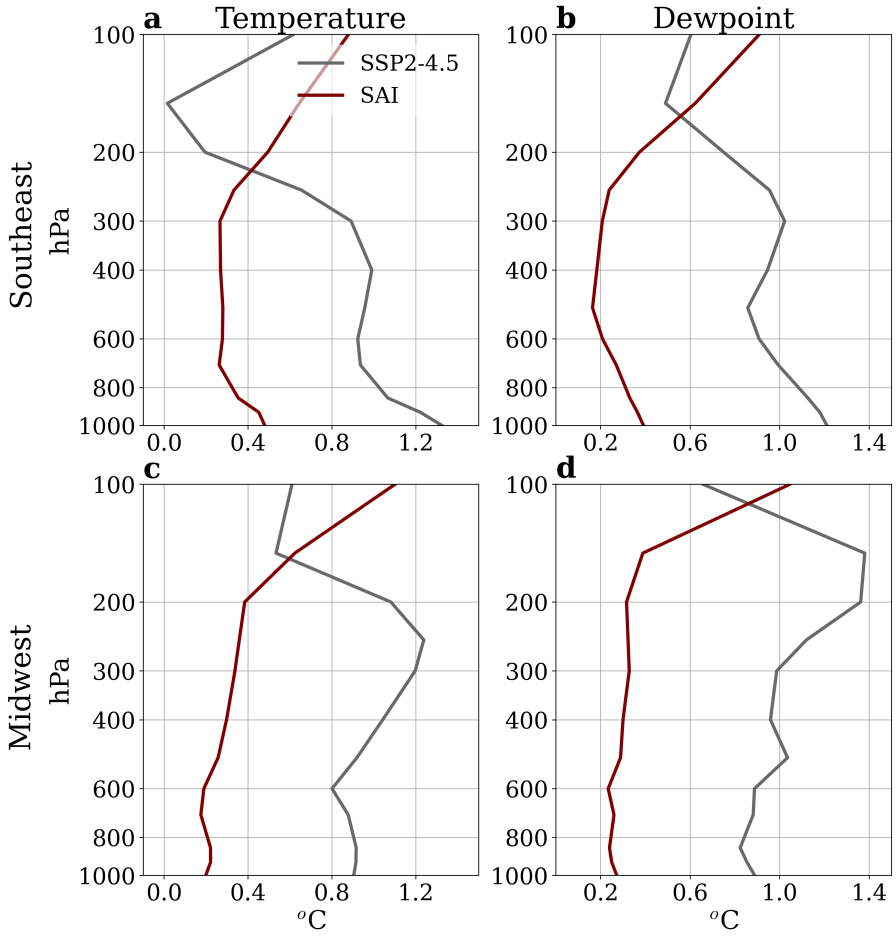

Figure 13 : Ensemble mean changes in the vertical profiles of temperature (a and c) and dew point (b and d) over the Midwest in JJA and the Southeast in MAM for 2060-2069 relative to 2015-2034. The SSP2-4.5 simulations are shown in gray and the SAI simulations are shown in red.

Future differences in tropospheric wind shear are more difficult to understand than SAI-induced changes in thermodynamic parameters. Under climate change with and without SAI, S06 is expected to decrease across much of the convectively active regions in the U.S. in the spring and summer seasons (Figure 6c, 6g, 7c, 7g). Although the decreases are small in magnitude relative to the climatology (Figure 5c, 5g), similar decreases have been documented in other studies of future climate change. Trapp et al. (2007), for instance, concluded that future decreases in tropospheric wind shear are consistent with decreases in the middle latitude thermal wind, as would be expected as the equator-to-pole temperature gradient decreases over the 21st century (Cohen et al., 2014; Francis & Vavrus, 2012). However, changes in S06 with SAI are broadly consistent with those in the no-SAI simulations examined here (Figure 6c, 6g, 7c, 7g), even though ARISE-SAI is configured so that the equator-to-pole temperature gradient remains near its 2035 value when SAI is deployed (Richter et al., 2022).

While a thorough analysis of these changes in wind shear are beyond the scope of this study, we do note that precipitation is projected to increase over the eastern equatorial Pacific during the seasons examined here under both the SAI and no-SAI simulations, although the increases projected with SAI are smaller in magnitude (Figure 14; see also Richter et al., 2022). Simpson et al. (2019) also indicated that precipitation is projected to increase in magnitude in the eastern equatorial Pacific in a future with SAI. Further, they examined the precipitation response to the addition of stratospheric heating in the absence of a greenhouse gas forcing, and found that precipitation is also projected to increase in the eastern equatorial Pacific. This suggests that precipitation changes in this region are influenced by dynamical responses that may result from the introduction of aerosols into the stratosphere. Upper-level divergence due to tropical convective heating in the equatorial Pacific can be the source of anomalous vorticity that drives the propagation of Rossby wave trains that impact the extratropics (Qin & Robinson, 1993; Sardeshmukh & Hoskins, 1988). This idea is broadly consistent with the spatial patterns of 300 hPa winds in both the SAI and no-SAI simulations, with alternating bands of increasing and decreasing winds emanating from the tropical eastern Pacific (Figure 15). In other words, future

changes in S06 in the SAI and no-SAI simulations may be driven by changes in tropical precipitation and associated large-scale climate circulations, which are similar whether or not SAI is deployed.

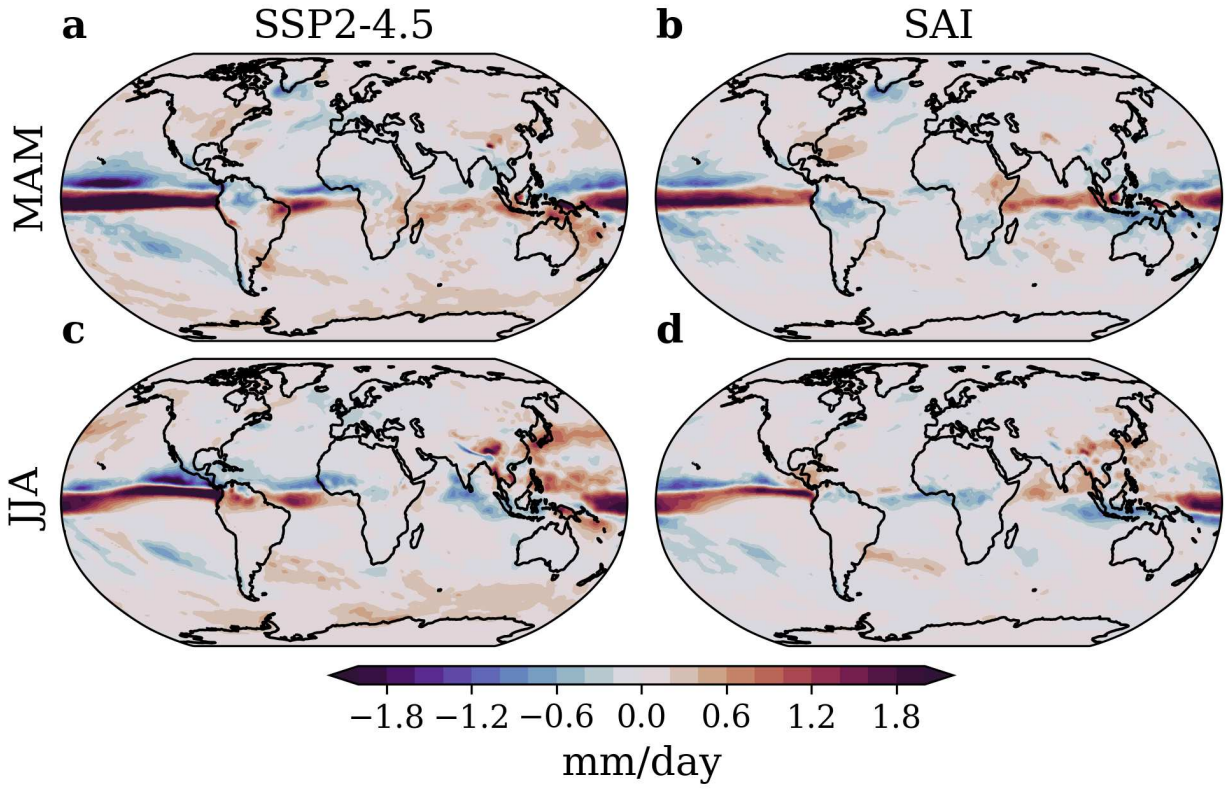

Figure 14 : Ensemble mean change in precipitation (2060-2069 relative to 2015-2034) for the SSP2-4.5 and SAI simulations during the boreal spring and summer seasons.

A novel aspect of this study is the use of individual ensemble members to examine the variability around the forced responses to climate change and SAI in large-scale convective weather environment parameters relevant to severe weather (Figure 11). Recall that each individual ensemble member represents an equally-plausible climate outcome in the decades ahead (e.g., Deser, 2020). Our results illustrate the large role internal climate variability will likely have, especially on regional scales. This large role also means that future convective weather environments in an SAI world could be indistinguishable from a world without SAI, even though the forced responses are distinguishable. We note that a 10-member ensemble is likely

insufficient to statistically capture the full breadth of possible outcomes (Deser et al., 2012; Franke et al., 2023). There are also shortcomings in the ability of Earth-system models to accurately represent internal variability (Orbe et al., 2020; O'Reilly et al., 2021).

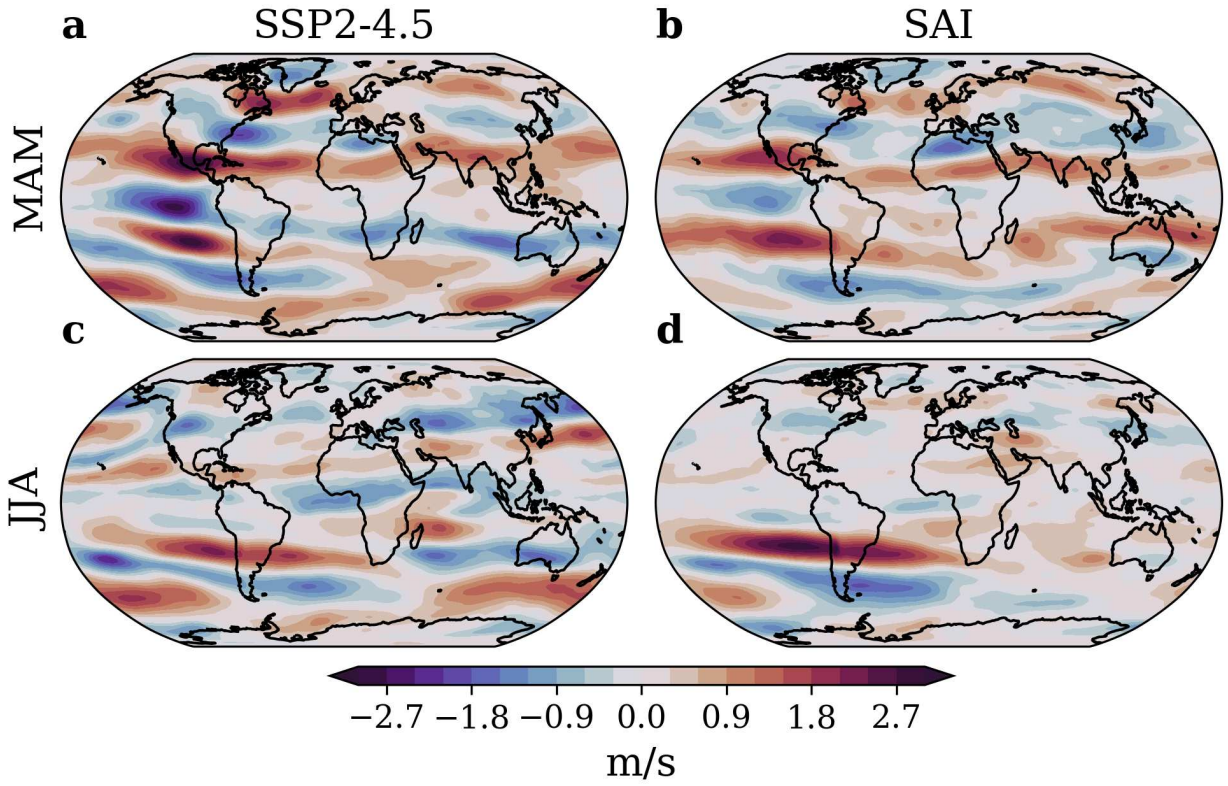

Figure 15 : Ensemble mean change in 300 hPa wind speed (2060-2069 relative to 2015-2034) for the SSP2-4.5 and SAI simulations during the boreal spring and summer seasons.

Other limitations of this study include the fact that the use of large-scale parameters to assess how the behavior of severe weather may change in the future is itself a caveat, since a favorable environment does not imply that convection will actually occur. Further, this method assumes that the frequency of convective initiation will not change with climate warming (Hoogewind et al., 2017; Trapp et al., 2007, 2009), and that the rate of initiation would not be affected by SAI deployment. Convective initiation is dependent on a variety of factors such as orography and large-scale dynamics, the latter of which have the potential to be impacted by

climate warming and potential SAI deployment. The representation of convective initiation is also likely sensitive to model configuration (Carlson et al., 1983; Trapp et al., 2007).

Finally, our analysis is based on a single model; namely CESM2-WACCM6. While it is a state-of-the-science Earth-system model that is improved over earlier versions, biases remain, for instance in the spatial distribution of tropical rainfall (Danabasoglu et al., 2020; Simpson et al., 2020; Wei et al., 2021). Future work could examine how model-specific biases impact future projections of convective weather environments with and without SAI. For instance, the exact ARISE-SAI scenarios examined here were recently completed using the first version of the U.K. Earth System Model (Archibald et al., 2020; Sellar et al., 2019). Ultimately, it will also be important to examine Earth system model simulations with different SAI deployment goals and timelines (e.g., MacMartin et al., 2022) or simulations under different climate change scenarios, such as the Stratospheric Aerosol Geoengineering Large Ensemble Project (Tilmes et al., 2018). It would also be interesting to use the output from Earth-system models to force high-resolution, regional climate models to explicitly examine how projected changes in the large-scale environment impact the distribution of convective modes (Ashley et al., 2023; Gensini et al., 2023; Gensini & Mote, 2015; Rasmussen et al., 2020; Trapp et al., 2019).

CHAPTER 5: ARISE-SAI-UKESM1.0 AND GLENS

5.1 Model Information and Introduction

Another ensemble of simulations that utilized the ARISE-SAI protocol were recently completed using the first version of the U.K. Earth-system Model (UKESM1.0) (Sellar et al., 2019). The atmospheric component of the UKESM1.0 is the United Kingdom Chemistry and Aerosol Model (UKCA), a high-top model with 85 vertical levels that extend from the surface to 85 km and a horizontal resolution of 1.875° longitude and 1.25° latitude (Archibald et al., 2020). The ARISE-SAI simulations with UKESM1.0 include five no-SAI ensemble members which span from 2015-2100 and five SAI ensemble members which span from 2035-2069. In this chapter we denote these simulations as ARISE-SAI-UKESM1.0 and we use ARISE-SAI to denote the CESM2 simulations that were discussed in the previous chapter.

Also, the Stratospheric Aerosol Geoengineering Large Ensemble (GLENS) project (Tilmes et al., 2018) is another set of parallel simulations of climate change with and without SAI that follows the Representative Concentration Pathway 8.5 (RCP8.5) emissions scenario, a high emissions scenario with little to no mitigation (van Vuuren et al., 2011). These simulations were run using the Community Earth System Model, version 1 (Hurrell et al., 2013). GLENS utilizes WACCM version 5, the high-top atmospheric component of CESM that includes a well-represented stratosphere. WACCM5 has 70 vertical levels extending from the surface to $\sim$140 km and has a horizontal resolution of 1.5° longitude and 0.9° latitude (Marsh et al., 2013; Mills et al., 2017). GLENS features the same controller as ARISE-SAI and maintains global-mean surface temperature, the interhemispheric temperature gradient and the pole-to-pole temperature gradient near their 2020 values ($\sim$1.2°C above pre-industrial levels) via the injection of SO_2 into the stratosphere (Kravitz et al., 2017; MacMartin et al., 2014). We focus on three ensemble members from GLENS with no-SAI that run from 2010-2097 and three ensemble members with SAI that run from 2020-2099. There are additional ensemble members in GLENS,

but they do not have the output necessary to calculate the convective weather environment parameters examined here.

The ARISE-SAI-UKESM1.0 and GLENS ensembles present an opportunity to increase understanding of how the model and scenario used affects how climate change and SAI impact convective weather environments over the U.S. In particular, ARISE-SAI-UKESM1.0 is useful because it provides the opportunity to compare directly to the ARISE-SAI simulations, potentially highlighting inter-model differences and sensitivities. By utilizing the RCP8.5 emissions scenario, GLENS provides insight into how convective weather environments might be impacted by a worst-case climate change scenario and a correspondingly aggressive SAI-deployment scenario. Differences in projections of annual mean near-surface (2 m) temperature in each of the simulations begin to illustrate some of these issues (Figure 16). For instance, even though ARISE-SAI and ARISE-SAI-UKESM1.0 were run under identical climate change and SAI deployment scenarios, CONUS mean near-surface temperature is $\sim$2°C cooler in UKESM1.0, and a slight reduction in temperature occurs shortly after deployment begins (Figure 16). This is because global mean near-surface temperature in ARISE-SAI-UKESM1.0 exceeds 1.5°C above the pre-industrial temperature before SAI deployment begins in 2035, likely due to its stronger equilibrium climate sensitivity relative to CESM2 (Meehl et al., 2020). Thus, SAI injections do not stabilize the global mean temperature as in ARISE-SAI, but rather must cool it for the first decade or so after deployment. In GLENS, temperature increases more rapidly than in the ARISE scenario (Figure 16), due to the higher greenhouse gas emissions in RCP8.5 relative to SSP2-4.5.

5.2 ARISE-SAI-UKESM1.0

In the simulations of ARISE-SAI-UKESM1.0, future increases in CAPE, CIN, and CAPES06 due to climate change have the potential to be avoided with SAI deployment (Figure 17). This signal, however, is less evident in ARISE-SAI-UKESM1.0 than in ARISE-SAI, perhaps because there are fewer ensemble members, which leads to a noisier response relative to ARISE-SAI (Figure 4, 17). We note that CAPE, CIN, and CAPES06 decrease slightly before

stabilizing in the SAI simulations, since UKESM1.0 is above the 1.5°C target when SAI is deployed (e.g., Figure 16). Similar to ARISE-SAI, S06 decreases throughout the time period in the no-SAI simulations in the Southeast and Midwest (Figure 4c, 4g, 17c, 17g). When SAI is deployed, S06 is projected to decrease as in the no-SAI simulations in the spring, but S06 decreases less in the summer with SAI relative to the simulations with no-SAI (Figure 17c, 17g).

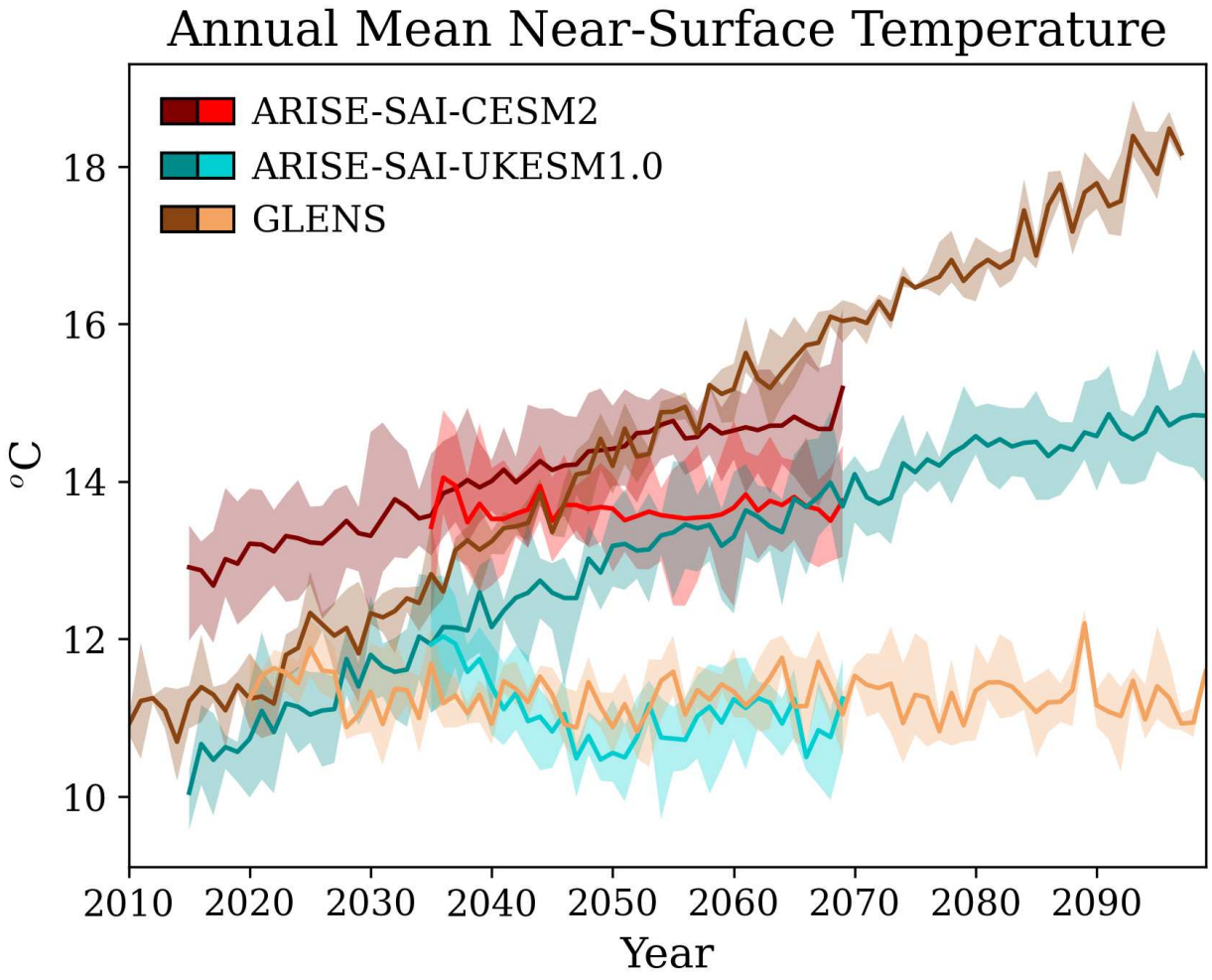

Figure 16 : CONUS mean temperature for ARISE-SAI (red), ARISE-SAI-UKESM1.0 (blue), and GLENS (brown) with and without SAI. Simulations with climate change only are represented by the dark colors and simulations with SAI deployment are represented by the lighter colors. ARISE-SAI-CESM2 and ARISE-SAI-UKESM1.0 run from 2015-2069 with SAI deployment beginning in 2035. GLENS runs from 2010-2099 with SAI deployment beginning in 2020. The shading represents the maximum and minimum range of the ensemble members and the solid line is representative of the ensemble mean.

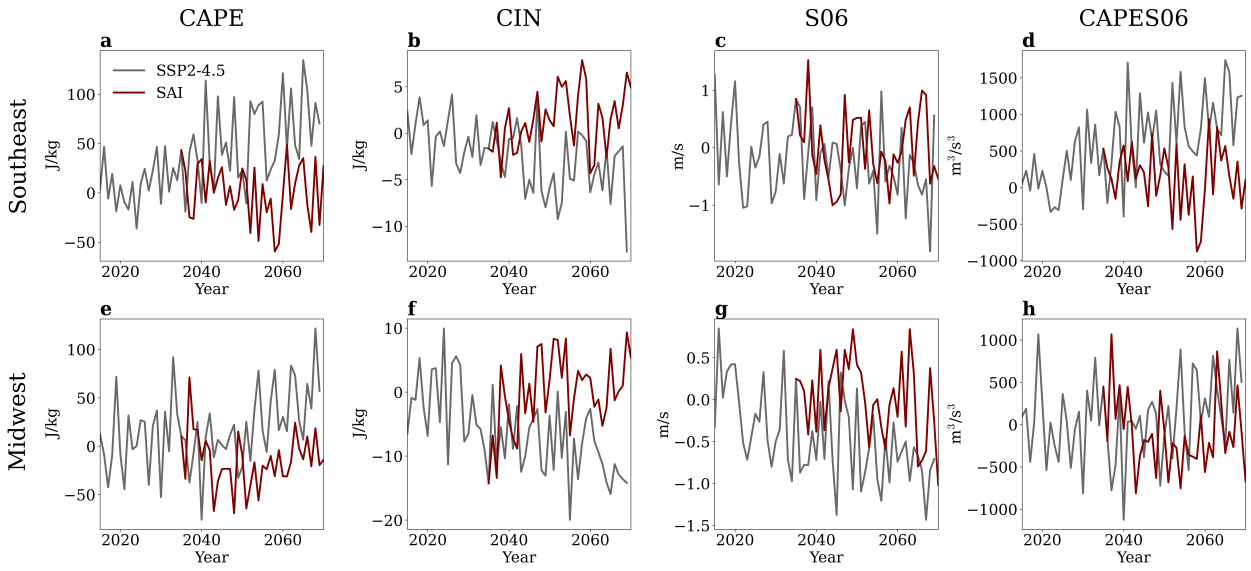

Figure 17 : CAPE, CIN, S06, and CAPES06 anomalies relative to the 2015-2034 mean in the Southeast in MAM (a-d) and the Midwest in JJA (e-h) for the ARISE-SAI-UKESM1.0 simulations. The red line represents the ensemble mean of the SAI simulations and runs from 2035-2069. The gray line represents the ensemble mean of the SSP2-4.5 simulations and runs from 2015-2069.

The climatology of CAPE, CIN, S06 and CAPES06 in ARISE-SAI-UKESM1.0 has a similar spatial distribution to ARISE-SAI in the spring and summer (Figure 3, 18). The magnitude of the 2015-2034 climatologies of CAPE, CIN, and CAPES06 are lower in ARISE-SAI-UKESM1.0 than in ARISE-SAI, and this is consistent with this model's lower temperatures across the CONUS (Figure 16). In the no-SAI simulations, CAPE, CIN and CAPES06 are projected to increase in magnitude in the spring and summer, with the largest increases occurring where magnitudes are largest climatologically (Figure 19). In the simulations with SAI, these increases are mostly avoided (Figure 20), as in ARISE-SAI (Figure 7).

S06 is projected to decrease in the simulations with no-SAI in the spring and summer across much of the U.S. in ARISE-SAI-UKESM1.0 (Figure 19c, 19g), as in ARISE-SAI (Figure 6c, 6g). When SAI is deployed, S06 is still projected to decrease across the northern two-thirds of the U.S. in the spring, but increase in magnitude in the southern U.S., especially along the Gulf Coast (Figure 20c). In the summer, projected decreases in S06 in the no-SAI simulations are mostly avoided, and S06 is projected to increase slightly in magnitude in some regions of the western

U.S. (Figure 20g). The difference between the SAI and no-SAI simulations indicates that S06 will be larger in magnitude in the simulations with SAI relative to the no-SAI simulations in the spring and summer (Figure 21c, 21g). To further understand changes in S06 in ARISE-SAI-UKESM1.0 both with and without SAI and how these changes differ from those projected in ARISE-SAI, changes in global precipitation and 300 hPa wind speed were examined.

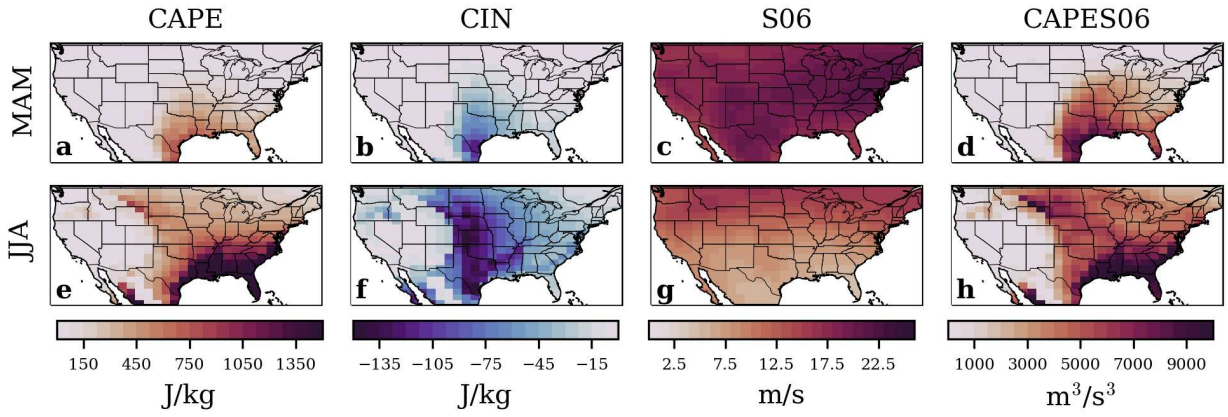

Figure 18 : 2015-2034 ensemble mean CAPE (a and e), CIN (b and f), S06 (c and g) and CAPES06 (d and h) for MAM (top row) and JJA (bottom row) in the SSP2-4.5 simulations in ARISE-SAI-UKESM1.0.

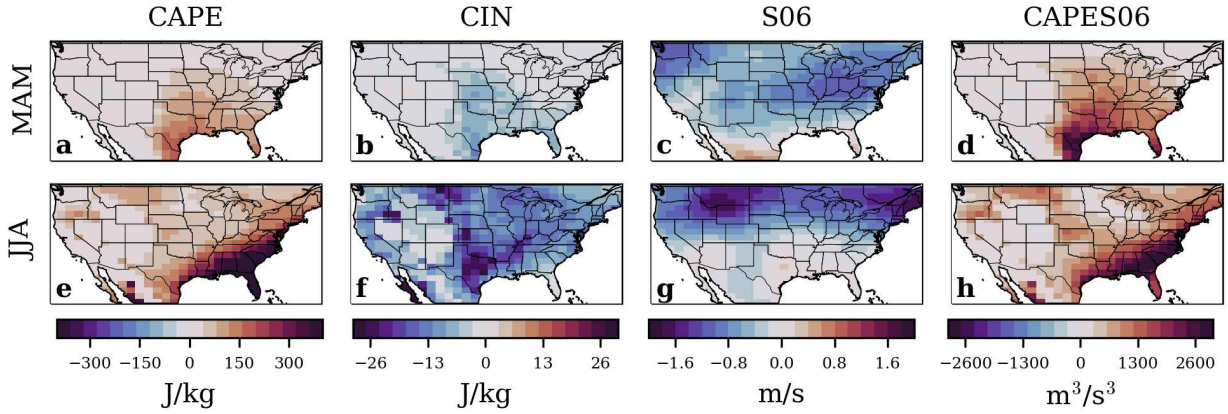

Figure 19 : The difference between the 2060-2069 (SSP2-4.5) and 2015-2034 (SSP2-4.5) ensemble mean CAPE, CIN, S06, and CAPES06 in MAM (top row) and JJA (bottom row) in ARISE-SAI-UKESM1.0.

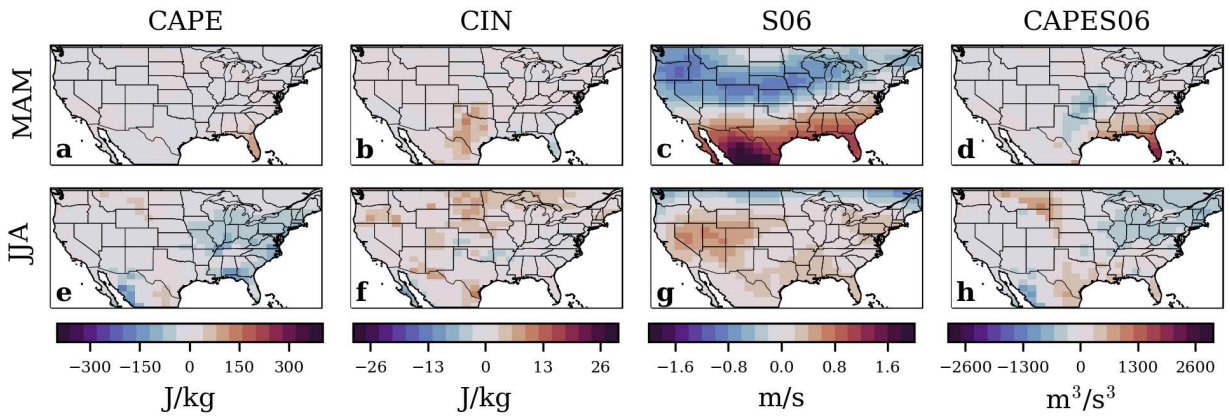

Figure 20 : The difference between the 2060-2069 (SAI) and 2015-2034 (SSP2-4.5) ensemble mean CAPE, CIN, S06, and CAPES06 in MAM (top row) and JJA (bottom row) in ARISE-SAI-UKESM1.0.

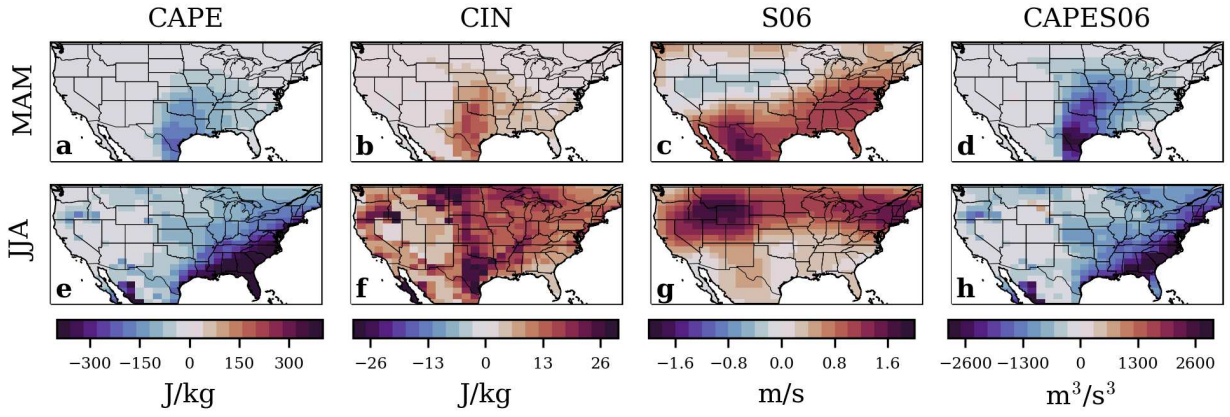

Figure 21 : The difference between SAI and SSP2-4.5 for the 2060-2069 ensemble mean in MAM (top row) and JJA (bottom row) in ARISE-SAI-UKESM1.0.

ARISE-SAI-UKESM1.0 projects that precipitation in the equatorial Pacific will increase in the simulations with no-SAI (Figure 22a, 22c) , similar to in ARISE-SAI (Figure 14a, 14c). When SAI is deployed, these increases are smaller in magnitude in the spring and are very small in the summer, and the spatial pattern of these changes differs between the SAI and no-SAI simulations (Figure 22b, 22d). Because the changes in precipitation are not as similar in the SAI and no-SAI simulations in ARISE-SAI-UKESM1.0 as in ARISE-SAI in both magnitude and spatial pattern (Figure 14, 22), it is likely that the resulting changes in the Rossby wave train pattern will be

distinct in the SAI and no-SAI simulations in ARISE-SAI-UKESM1.0. Changes in 300hPa wind speed over this same time period with SAI are characterized by alternating bands of increasing and decreasing wind speeds that are slightly phase-shifted relative to the no-SAI simulations in the spring, and are even more phase-shifted from the no-SAI simulations in the summer, when 300 hPa wind speed is projected to increase across much of the U.S. (Figure 23).

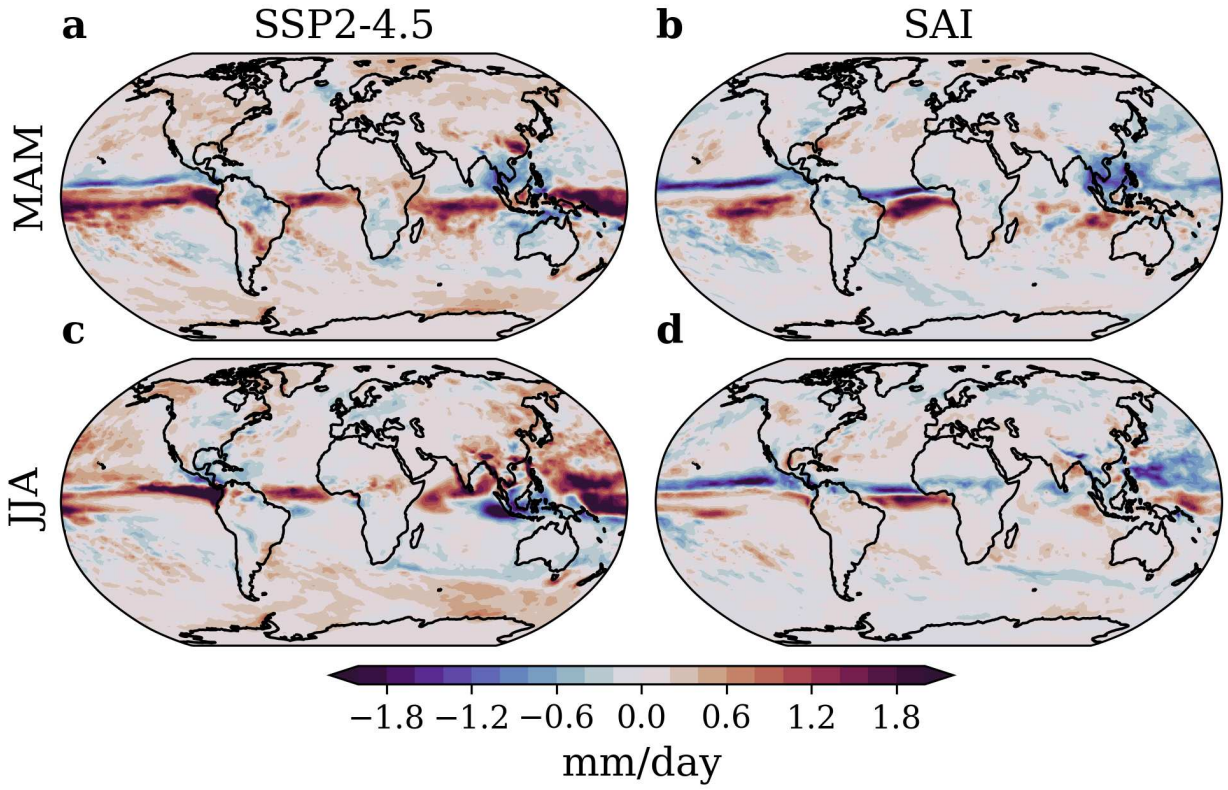

Figure 22 : Ensemble mean change in precipitation (2060-2069 relative to 2015-2034) for the SSP2-4.5 and SAI simulations during the boreal spring and summer seasons in ARISE-SAI-UKESM1.0

In ARISE-SAI-UKESM1.0, the difference between the SAI and no-SAI simulations for bivariate distribution of CAPE and CIN over 2060-2069 is similar to that in ARISE-SAI in the Southeast and Midwest, where there are fewer days with high magnitude CAPE and CIN and more days with moderate CAPE and CIN in the SAI simulations (Figure 9, 24). One difference is that in both the SAI and no-SAI simulations, the range of CAPE and CIN magnitudes are smaller in ARISE-SAI-UKESM1.0 than in ARISE-SAI, likely due to lower temperatures across the U.S.

in UKESM1.0 (Figure 16) relative to CESM2 (Figure 16). The difference between SAI and no-SAI simulations for the bivariate distribution of CAPE and S06 indicate that there will be fewer days with high magnitude CAPE in the SAI simulations across the Southeast, and that this shift will be independent of the magnitude of S06 in ARISE-SAI-UKESM1.0, as in ARISE-SAI (Figure 10a, 25a). In contrast to ARISE-SAI, there will be fewer days with low magnitude S06 in the Midwest in the simulations with SAI compared to the simulations with no-SAI in ARISE-SAI-UKESM1.0 (Figure 25b). This shift is in agreement with projections of changes in S06 over the simulation period, where projected decreases in S06 in the no-SAI simulations in the summer are avoided across much of the U.S. (Figure 19g, 20g).

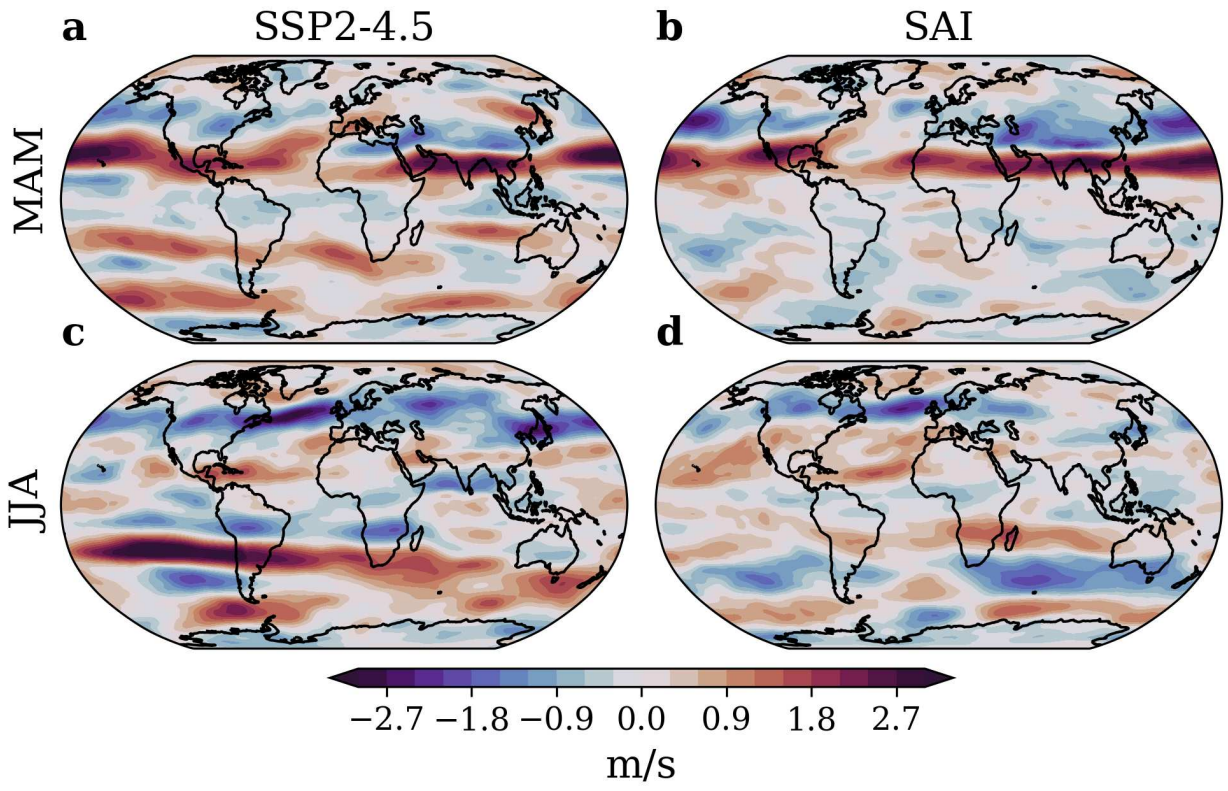

Figure 23 : Ensemble mean change in 300 hPa wind speed (2060-2069 relative to 2015-2034) for the SSP2-4.5 and SAI simulations during the boreal spring and summer seasons in ARISE-SAI-UKESM1.0

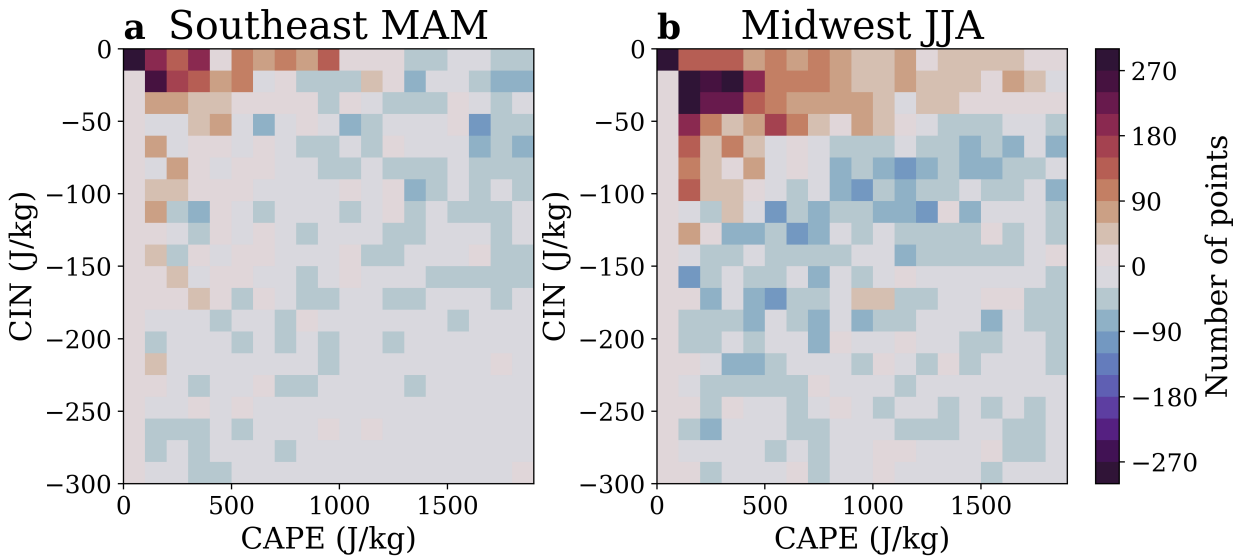

Figure 24 : The difference between the SAI and no-SAI simulations (i.e. SAI - SSP2-4.5) for the bivariate distribution of CAPE (x-axis) and CIN (y-axis) for the Southeast in MAM (a) and the Midwest in JJA (b) over 2060-2069 in ARISE-SAI-UKESM1.0. Red (blue) pixels represent bins where there are more (less) days with corresponding CAPE and CIN values in the simulations with SAI.

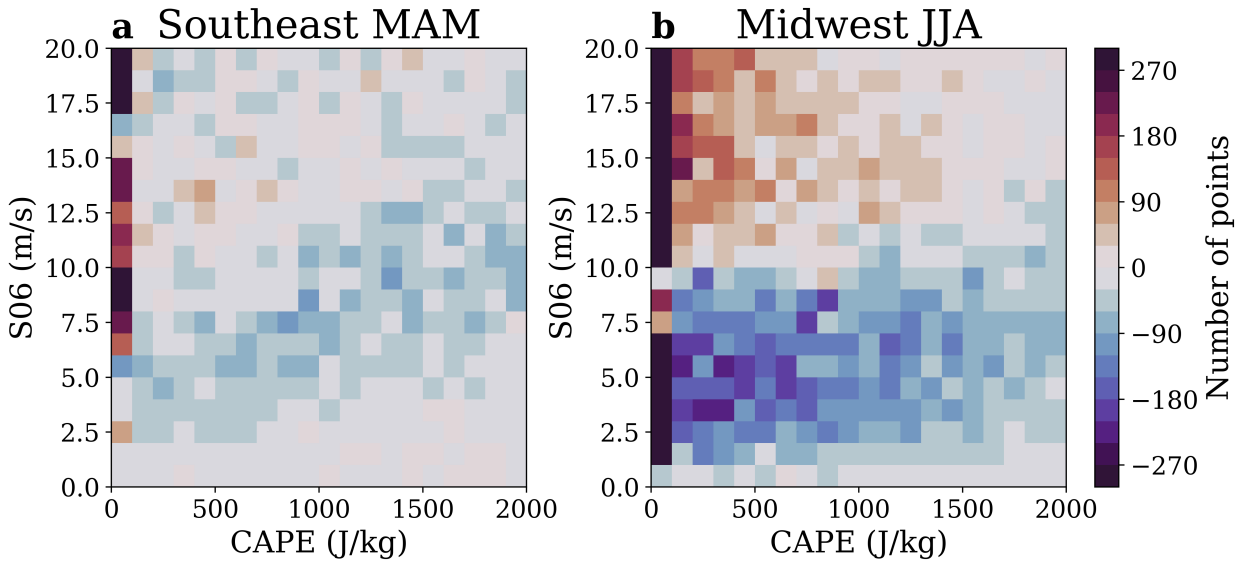

Figure 25 : The difference between the SAI and no-SAI simulations (i.e. SAI - SSP2-4.5) for the bivariate distribution of CAPE (x-axis) and S06 (y-axis) for the Southeast in MAM (a) and the Midwest in JJA (b) over 2060-2069 in ARISE-SAI-UKESM1.0. Red (blue) pixels represent bins where there are more (less) days with corresponding CAPE and CIN values in the simulations with SAI.

5.3 GLENS

Future changes in convective weather environment parameters in GLENS are analyzed by observing changes at the end of the simulation period (2080-2089) relative to the 2010-2019 mean. The GLENS simulations are useful to examine potential forced changes due to climate change with and without SAI because GLENS considers an extreme emissions scenario paired with an aggressive SAI deployment scenario, resulting in a high signal to noise ratio (Tilmes et al., 2018). This is evident when examining the time series of anomalies of CAPE, CIN, S06 and CAPES06 over the Southeast in MAM and the Midwest in JJA, where the stabilizing influence of SAI deployment on the magnitudes CAPE, CIN and CAPES06 is clearly evident (Figure 26).

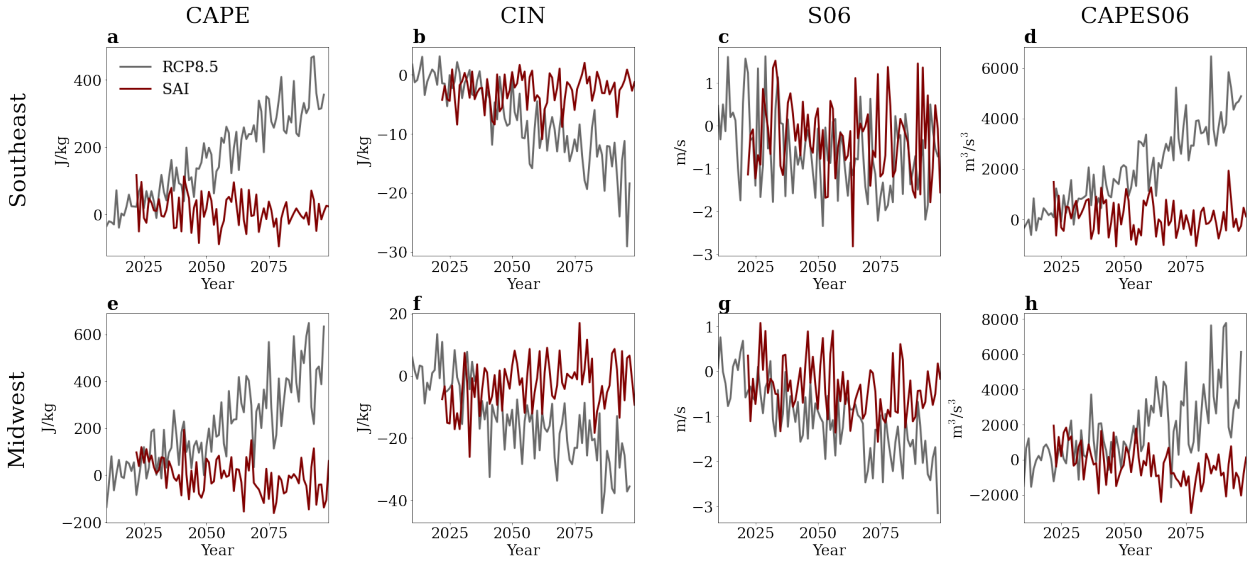

Figure 26 : CAPE, CIN, S06, and CAPES06 anomalies relative to the 2010-2019 mean in the Southeast in MAM (a-d) and the Midwest in JJA (e-h) for the GLENS simulations. The gray line represents the ensemble mean of the SSP2-4.5 simulations and runs from 2010-2097. The red line represents the ensemble mean of the SAI simulations and runs from 2020-2099.

The underlying climatology (2010-2019) of the convective weather environment parameters considered across the U.S. in the spring and summer is shown in Figure 27. Future changes in CAPE, CIN, and CAPES06 exhibit increased magnitudes due to climate change that are largely avoided by the deployment of SAI (Figure 28, 29, 30). In the SAI simulations, there will be fewer

days with high magnitude CAPE and CIN, and more days with moderate CAPE and CIN in the spring in GLENS, relative to the simulations with SAI (Figure 31a). In the summer, there will be fewer days with high magnitude CIN in the simulations with SAI, and this is largely independent of the magnitude of CAPE (Figure 31b). The difference in projections of CAPE, CIN and CAPES06 with and without SAI are likely driven by the avoidance of continued temperature increases in the simulations where SAI is deployed (Figure 16).

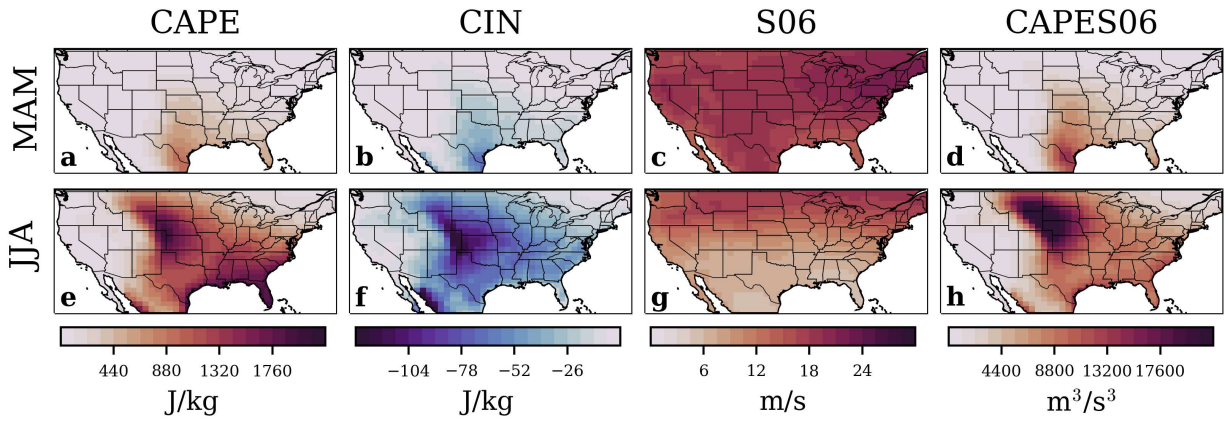

Figure 27 : 2010-2019 ensemble mean CAPE (a and e), CIN (b and f), S06 (c and g), and CAPES06 (d and h) for MAM (top row) and JJA (bottom row) for the RCP8.5 simulations in GLENS.

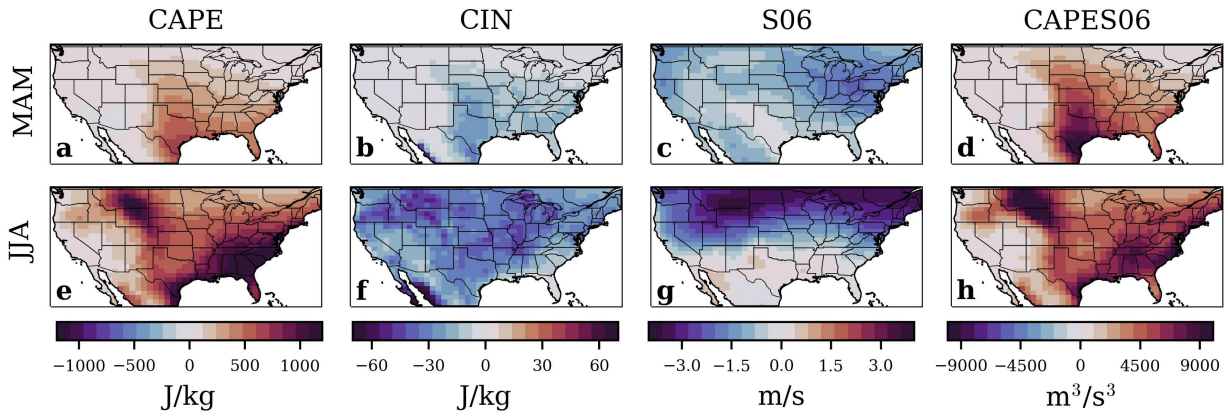

Figure 28 : The difference between the 2080-2089 (RCP8.5) and 2010-2019 (RCP8.5) ensemble mean CAPE, CIN, S06, and CAPES06 in MAM (top row) and JJA (bottom row) in the GLENS simulations.

In GLENS, S06 is projected to decrease less in the simulations with SAI than in the simulations with no-SAI in the spring and summer (Figure 28c, 28g, 29c, 29g). These differences are especially apparent in the summer (Figure 30g). In the spring, there will be fewer days with high magnitude CAPE with SAI compared to the simulations with no-SAI in GLENS (Figure 32a). In the summer, there will be fewer days with low magnitude S06 in the simulations with SAI in GLENS (Figure 32b). The difference in the shift in the bivariate distribution of CAPE and S06 in the SAI and no-SAI simulations in the spring and summer could be because in the spring, there is little difference in S06 between the no-SAI and SAI simulations in the Southeast, and so the shift is dominated by decreasing magnitude CAPE in the SAI simulations (Figure 32a, 32c). In the summer, the magnitude of S06 is larger in the simulations with SAI compared to the no-SAI simulations, especially across the northern half of the U.S., which includes much of the Midwest, indicating the potential for difference between the magnitude of S06 in the SAI and no-SAI simulations to play a more dominant role in the bivariate distribution of CAPE and S06 (Figure 30g).

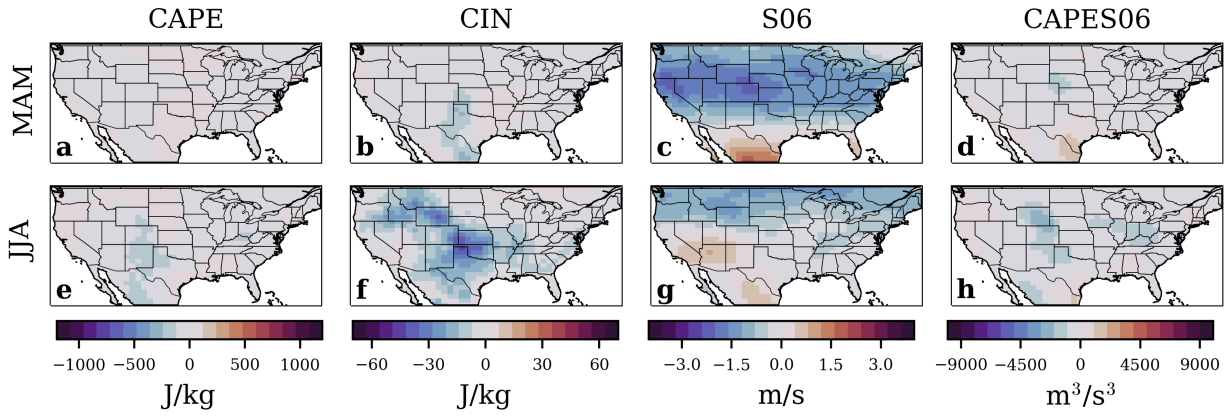

Figure 29 : The difference between the 2080-2089 (SAI) and 2010-2019 (RCP8.5) ensemble mean CAPE, CIN, S06, and CAPES06 in MAM (top row) and JJA (bottom row) in the GLENS simulations.

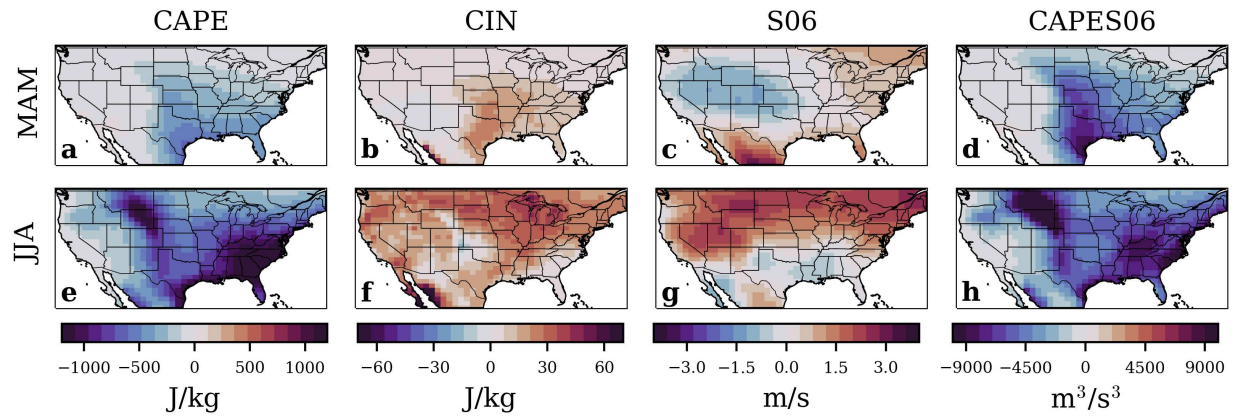

Figure 30 : The difference between SAI and RCP8.5 for the 2080-2089 ensemble mean in MAM (top row) and JJA (bottom row) in GLENS.

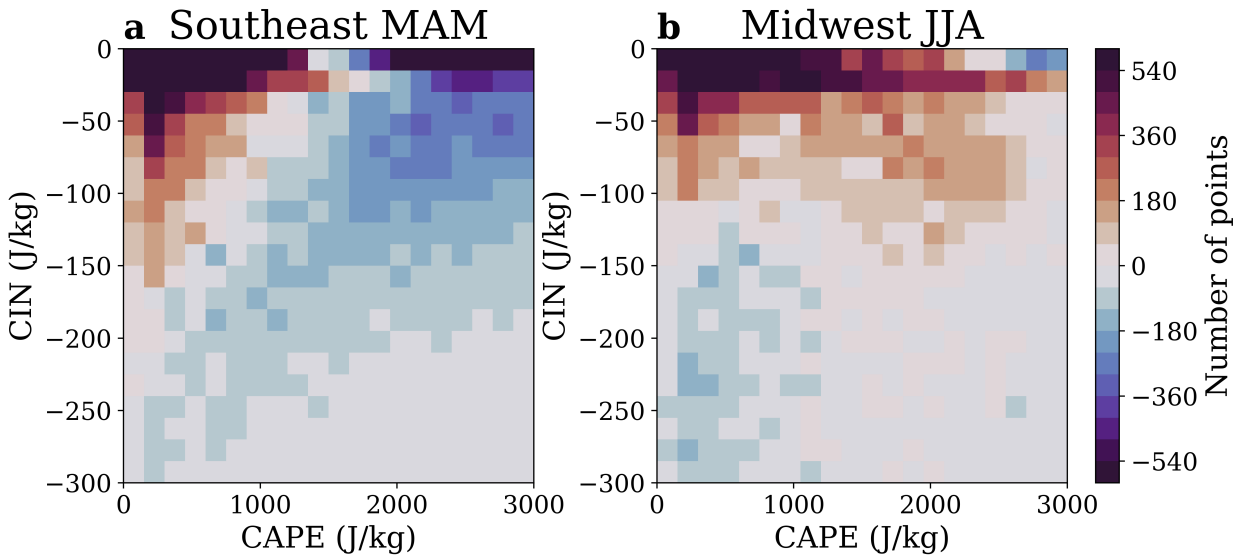

Figure 31 : The difference between the SAI and no-SAI simulations (i.e. SAI - RCP8.5) for the bivariate distribution of CAPE (x-axis) and CIN (y-axis) for the Southeast in MAM (a) and the Midwest in JJA (b) over 2080-2089 in GLENS. Red (blue) pixels represent bins where there are more (less) days with corresponding CAPE and CIN values in the simulations with SAI.

5.4 Conclusion

Forced changes of CAPE, CIN, S06, and CAPES06 in the no-SAI simulations in ARISE-SAI-UKESM1.0 are largely similar to those projected by ARISE-SAI and are in general agreement with previous literature (Figure 6, 19) (Diffenbaugh et al., 2013; Franke et al., 2023;

Hoogewind et al., 2017; Rasmussen et al., 2020; Seeley & Romps, 2015; Trapp et al., 2007). Forced changes of CAPE, CIN and CAPES06 in the simulations where SAI is deployed are generally similar across the two models (Figure 7, 20). Projected changes in S06 differ from ARISE-SAI in the simulations with SAI, especially in the summer, where S06 is projected to be larger in the simulations with SAI compared to the no-SAI simulations especially in the northern half of the U.S. (Figure 6c, 6g). The differences in future projections of S06 in both models have been linked to differences in projections of precipitation change in the equatorial Pacific (Figure 14, 22).

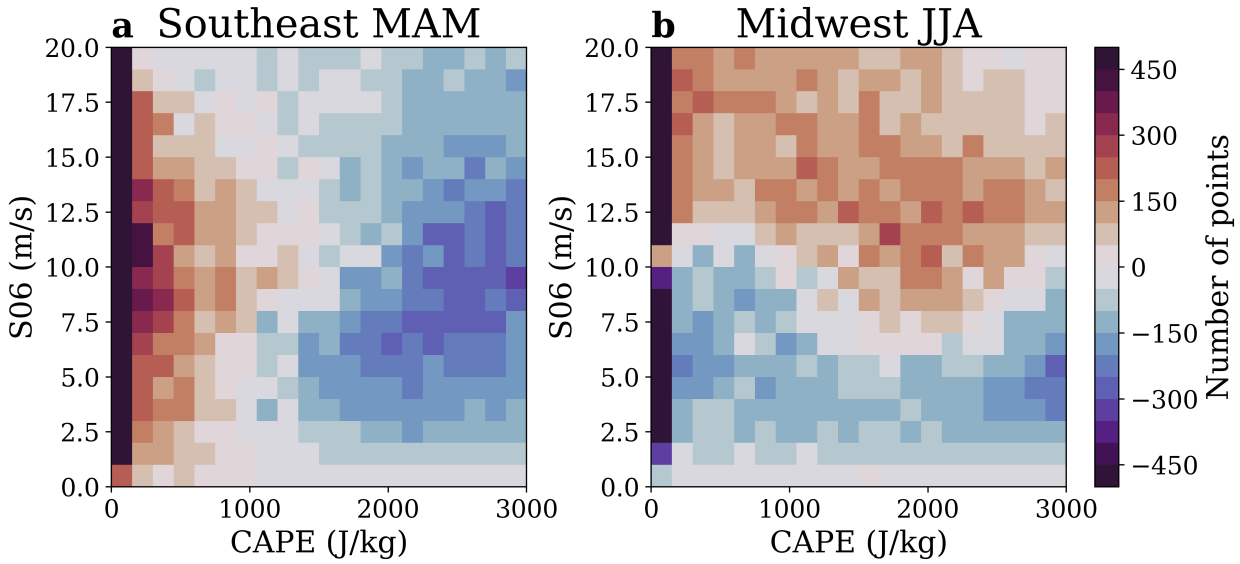

Figure 32 : The difference between the SAI and no-SAI simulations (i.e. SAI - RCP8.5) for the bivariate distribution of CAPE (x-axis) and S06 (y-axis) for the Southeast in MAM (a) and the Midwest in JJA (b) over 2080-2089 in GLENS. Red (blue) pixels represent bins where there are more (less) days with corresponding CAPE and CIN values in the simulations with SAI.

Analysis of future changes of convective weather environment parameters in GLENS provide more evidence for the potential of SAI deployment to stabilize CAPE, CIN, and CAPES06 magnitudes similar to how annual mean near-surface temperature is stabilized (Figure 16); in particular, with more climate change and stronger SAI deployment to counter it, future projections of these parameters are very distinct in GLENS simulations with and without SAI (Figure 26). Projected changes in S06 indicate that future decreases in S06 in the no-SAI

simulations could be lessened with SAI deployment (Figure 28c, 28g, 29c, 29g). Future work could investigate if these changes are linked to changes in tropical precipitation, as was done for ARISE-SAI and ARISE-SAI-UKESM1.0.

REFERENCES

Abiodun, B. J., Odoulami, R. C., Sawadogo, W., Oloniyo, O. A., Abatan, A. A., New, M., et al. (2021). Potential impacts of stratospheric aerosol injection on drought risk managements over major river basins in Africa. *Climatic Change*, 169(3), 31. https://doi.org/10.1007/s10584-021-03268-w

Allen, J. T., Molina, M. J., & Gensini, V. A. (2018). Modulation of Annual Cycle of Tornadoes by El Niño–Southern Oscillation. *Geophysical Research Letters*, 45(11), 5708–5717. https://doi.org/10.1029/2018GL077482

Allen, M. R., & Ingram, W. J. (2002). Constraints on future changes in climate and the hydrologic cycle. *Nature*, 419(6903), 224–232. https://doi.org/10.1038/nature01092

Archibald, A. T., O'Connor, F. M., Abraham, N. L., Archer-Nicholls, S., Chipperfield, M. P., Dalvi, M., et al. (2020). Description and evaluation of the UKCA stratosphere–troposphere chemistry scheme (StratTrop vn 1.0) implemented in UKESM1. *Geoscientific Model Development*, 13(3), 1223–1266. https://doi.org/10.5194/gmd-13-1223-2020

Ashley, W. S., Haberlie, A. M., & Gensini, V. A. (2023). The Future of Supercells in the United States. *Bulletin of the American Meteorological Society*, 104(1), E1–E21. https://doi.org/10.1175/BAMS-D-22-0027.1

Baggett, C. F., Nardi, K. M., Childs, S. J., Zito, S. N., Barnes, E. A., & Maloney, E. D. (2018). Skillful Subseasonal Forecasts of Weekly Tornado and Hail Activity Using the Madden-Julian Oscillation. *Journal of Geophysical Research: Atmospheres*, 123(22), 12,661-12,675. https://doi.org/10.1029/2018JD029059

Barnes, E. A., Hurrell, J. W., & Sun, L. (2022). Detecting Changes in Global Extremes Under the GLENS-SAI Climate Intervention Strategy. *Geophysical Research Letters*, 49(20), e2022GL100198. https://doi.org/10.1029/2022GL100198

Bednarz, E. M., Visioni, D., Richter, J. H., Butler, A. H., & MacMartin, D. G. (2022). Impact of the Latitude of Stratospheric Aerosol Injection on the Southern Annular Mode. *Geophysical Research Letters*, 49(19), e2022GL100353. https://doi.org/10.1029/2022GL100353

Brooks, H. E., Lee, J. W., & Craven, J. P. (2003). The spatial distribution of severe thunderstorm and tornado environments from global reanalysis data. *Atmospheric Research*, 67–68, 73–94. https://doi.org/10.1016/S0169-8095(03)00045-0

Brooks, H. E., Anderson, A. R., Riemann, K., Ebbers, I., & Flachs, H. (2007). Climatological aspects of convective parameters from the NCAR/NCEP reanalysis. *Atmospheric Research*, 83(2), 294–305. https://doi.org/10.1016/j.atmosres.2005.08.005

Carlson, T. N., Benjamin, S. G., Forbes, G. S., & Li, Y.-F. (1983). Elevated Mixed Layers in the Regional Severe Storm Environment: Conceptual Model and Case Studies. *Monthly Weather Review*, 111(7), 1453–1474. https://doi.org/10.1175/1520-0493(1983)111¡1453:EMLITR¿2.0.CO;2

Cohen, J., Screen, J. A., Furtado, J. C., Barlow, M., Whittleston, D., Coumou, D., et al. (2014). Recent Arctic amplification and extreme mid-latitude weather. *Nature Geoscience*, 7(9), 627–637. https://doi.org/10.1038/ngeo2234

Craven, J. P., & Brooks, H. E. (2004). BASELINE CLIMATOLOGY OF SOUNDING DERIVED PARAMETERS ASSOCIATED WITH DEEP MOIST CONVECTION. *National Weather Digest*, 28.

Crutzen, P. J. (2006). Albedo Enhancement by Stratospheric Sulfur Injections: A Contribution to Resolve a Policy Dilemma? *Climatic Change*, 77(3–4), 211. https://doi.org/10.1007/s10584-006-9101-y

Danabasoglu, G., Lamarque, J.-F., Bacmeister, J., Bailey, D. A., DuVivier, A. K., Edwards, J., et al. (2020). The Community Earth System Model Version 2 (CESM2). *Journal of Advances in Modeling Earth Systems*, 12(2), e2019MS001916.

https://doi.org/10.1029/2019MS001916

Deser, C. (2020). “Certain Uncertainty: The Role of Internal Climate Variability in Projections of Regional Climate Change and Risk Management.” *Earth’s Future*, 8(12), e2020EF001854. https://doi.org/10.1029/2020EF001854

Deser, C., Knutti, R., Solomon, S., & Phillips, A. S. (2012). Communication of the role of natural variability in future North American climate. *Nature Climate Change*, 2(11), 775–779. https://doi.org/10.1038/nclimate1562

Diffenbaugh, N. S., Scherer, M., & Trapp, R. J. (2013). Robust increases in severe thunderstorm environments in response to greenhouse forcing. *Proceedings of the National Academy of Sciences*, 110(41), 16361–16366. https://doi.org/10.1073/pnas.1307758110

Donat, M. G., Lowry, A. L., Alexander, L. V., O’Gorman, P. A., & Maher, N. (2016). More extreme precipitation in the world’s dry and wet regions. *Nature Climate Change*, 6(5), 508–513. https://doi.org/10.1038/nclimate2941

Doswell, C. A., & Rasmussen, E. N. (1994). The Effect of Neglecting the Virtual Temperature Correction on CAPE Calculations. *Weather and Forecasting*, 9(4), 625–629. https://doi.org/10.1175/1520-0434(1994)009¡0625:TEONTV¿2.0.CO;2

Doswell, C. A., Brooks, H. E., & Maddox, R. A. (1996). Flash Flood Forecasting: An Ingredients-Based Methodology. *Weather and Forecasting*, 11(4), 560–581. https://doi.org/10.1175/1520-0434(1996)011¡0560:FFFAIB¿2.0.CO;2

Doswell, C. A., Brooks, H. E., & Kay, M. P. (2005). Climatological Estimates of Daily Local Nontornadic Severe Thunderstorm Probability for the United States. *Weather and Forecasting*, 20(4), 577–595. https://doi.org/10.1175/WAF866.1

Eyring, V., Bony, S., Meehl, G. A., Senior, C. A., Stevens, B., Stouffer, R. J., & Taylor, K. E. (2016). Overview of the Coupled Model Intercomparison Project Phase 6 (CMIP6) experimental design and organization. *Geoscientific Model Development*, 9(5), 1937–1958. https://doi.org/10.5194/gmd-9-1937-2016

Francis, J. A., & Vavrus, S. J. (2012). Evidence linking Arctic amplification to extreme weather in

mid-latitudes. *Geophysical Research Letters*, 39(6). https://doi.org/10.1029/2012GL051000

Franke, M. E., Hurrell, J. W., Rasmussen, K., & Sun, L. (2023). Impacts of Forced and Internal Climate Variability on Changes in Convective Environments Over the Eastern United States (preprint). *Preprints*. https://doi.org/10.22541/essoar.167458066.68764316/v1

Friedlingstein, P., O'Sullivan, M., Jones, M. W., Andrew, R. M., Gregor, L., Hauck, J., et al. (2022). Global Carbon Budget 2022. *Earth System Science Data*, 14(11), 4811–4900. https://doi.org/10.5194/essd-14-4811-2022

Galway, J. G. (1989). The Evolution of Severe Thunderstorm Criteria within the Weather Service. *Weather and Forecasting*, 4(4), 585–592. https://doi.org/10.1175/1520-0434(1989)004¡0585:TEOSTC¿2.0.CO;2

Gensini, V. A., & Mote, T. L. (2015). Downscaled estimates of late 21st century severe weather from CCSM3. *Climatic Change*, 129(1), 307–321. https://doi.org/10.1007/s10584-014-1320-z

Gensini, V. A., Haberlie, A. M., & Ashley, W. S. (2023). Convection-permitting simulations of historical and possible future climate over the contiguous United States. Climate Dynamics, 60(1), 109–126. https://doi.org/10.1007/s00382-022-06306-0

Gettelman, A., Mills, M. J., Kinnison, D. E., Garcia, R. R., Smith, A. K., Marsh, D. R., et al. (2019). The Whole Atmosphere Community Climate Model Version 6 (WACCM6). *Journal of Geophysical Research: Atmospheres*, 124(23), 12380–12403. https://doi.org/10.1029/2019JD030943

Hawkins, E., & Sutton, R. (2009). The Potential to Narrow Uncertainty in Regional Climate Predictions. *Bulletin of the American Meteorological Society*, 90(8), 1095–1108. https://doi.org/10.1175/2009BAMS2607.1

Haywood, J. M., Jones, A., Johnson, B. T., & McFarlane Smith, W. (2022). Assessing the consequences of including aerosol absorption in potential stratospheric aerosol injection climate intervention strategies. *Atmospheric Chemistry and Physics*, 22(9), 6135–6150.

https://doi.org/10.5194/acp-22-6135-2022

Hoogewind, K. A., Baldwin, M. E., & Trapp, R. J. (2017). The Impact of Climate Change on Hazardous Convective Weather in the United States: Insight from High-Resolution Dynamical Downscaling. *Journal of Climate*, 30(24), 10081–10100. https://doi.org/10.1175/JCLI-D-16-0885.1

Hueholt, D. M., Barnes, E. A., Hurrell, J. W., Richter, J. H., & Sun, L. (2023). Assessing Outcomes in Stratospheric Aerosol Injection Scenarios Shortly After Deployment. *Earth's Future*, 11(5), e2023EF003488. https://doi.org/10.1029/2023EF003488

Hurrell, J. W., Holland, M. M., Gent, P. R., Ghan, S., Kay, J. E., Kushner, P. J., et al. (2013). The Community Earth System Model: A Framework for Collaborative Research. *Bulletin of the American Meteorological Society*, 94(9), 1339–1360. https://doi.org/10.1175/BAMS-D-12-00121.1

IPCC. (2021). Summary for Policymakers.

Ji, D., Fang, S., Curry, C. L., Kashimura, H., Watanabe, S., Cole, J. N. S., et al. (2018). Extreme temperature and precipitation response to solar dimming and stratospheric aerosol geoengineering. *Atmospheric Chemistry and Physics*, 18(14), 10133–10156. https://doi.org/10.5194/acp-18-10133-2018

Jiang, X., & Guan, D. (2016). Determinants of global CO2 emissions growth. *Applied Energy*, 184, 1132–1141. https://doi.org/10.1016/j.apenergy.2016.06.142

Kay, J. E., Deser, C., Phillips, A., Mai, A., Hannay, C., Strand, G., et al. (2015). The Community Earth System Model (CESM) Large Ensemble Project: A Community Resource for Studying Climate Change in the Presence of Internal Climate Variability. *Bulletin of the American Meteorological Society*, 96(8), 1333–1349. https://doi.org/10.1175/BAMS-D-13-00255.1

Kelly, D. L., Schaefer, J. T., & Doswell, C. A. (1985). Climatology of Nontornadic Severe Thunderstorm Events in the United States. *Monthly Weather Review*, 113(11), 1997–2014. https://doi.org/10.1175/1520-0493(1985)113¡1997:CONSTE¿2.0.CO;2

Keys, P. W., Barnes, E. A., Diffenbaugh, N. S., Hurrell, J. W., & Bell, C. M. (2022). Potential for perceived failure of stratospheric aerosol injection deployment. *Proceedings of the National Academy of Sciences*, 119(40), e2210036119. https://doi.org/10.1073/pnas.2210036119

Kravitz, B., Robock, A., Tilmes, S., Boucher, O., English, J. M., Irvine, P. J., et al. (2015). The Geoengineering Model Intercomparison Project Phase 6 (GeoMIP6): simulation design and preliminary results. *Geoscientific Model Development*, 8(10), 3379–3392. https://doi.org/10.5194/gmd-8-3379-2015

Kravitz, B., Robock, A., Boucher, O., Schmidt, H., Taylor, K. E., Stenchikov, G., & Schulz, M. (2011). The Geoengineering Model Intercomparison Project (GeoMIP). *Atmospheric Science Letters*, 12(2), 162–167. https://doi.org/10.1002/asl.316

Kravitz, B., MacMartin, D. G., Mills, M. J., Richter, J. H., Tilmes, S., Lamarque, J.-F., et al. (2017). First Simulations of Designing Stratospheric Sulfate Aerosol Geoengineering to Meet Multiple Simultaneous Climate Objectives. Journal of Geophysical Research: Atmospheres, 122(23), 12,616-12,634. https://doi.org/10.1002/2017JD026874

Lee, W. R., MacMartin, D. G., Visioni, D., Kravitz, B., Chen, Y., Moore, J. C., et al. (2023). High-Latitude Stratospheric Aerosol Injection to Preserve the Arctic. *Earth's Future*, 11(1), e2022EF003052. https://doi.org/10.1029/2022EF003052

Lepore, C., Abernathey, R., Henderson, N., Allen, J. T., & Tippett, M. K. (2021). Future Global Convective Environments in CMIP6 Models. *Earth's Future*, 9(12), e2021EF002277. https://doi.org/10.1029/2021EF002277

Li, F., Chavas, D. R., Reed, K. A., & Ii, D. T. D. (2020). Climatology of Severe Local Storm Environments and Synoptic-Scale Features over North America in ERA5 Reanalysis and CAM6 Simulation. *Journal of Climate*, 33(19), 8339–8365. https://doi.org/10.1175/JCLI-D-19-0986.1

Lockley, A., MacMartin, D., & Hunt, H. (2020). An update on engineering issues concerning stratospheric aerosol injection for geoengineering. *Environmental Research*

Communications, 2(8), 082001. https://doi.org/10.1088/2515-7620/aba944

MacMartin, D. G., Visioni, D., Kravitz, B., Richter, J. H., Felgenhauer, T., Lee, W. R., et al. (2022). Scenarios for modeling solar radiation modification. *Proceedings of the National Academy of Sciences*, 119(33), e2202230119. https://doi.org/10.1073/pnas.2202230119

MacMartin, D. G., Kravitz, B., Keith, D. W., & Jarvis, A. (2014). Dynamics of the coupled human–climate system resulting from closed-loop control of solar geoengineering. *Climate Dynamics*, 43(1), 243–258. https://doi.org/10.1007/s00382-013-1822-9

Marsh, D. R., Mills, M. J., Kinnison, D. E., Lamarque, J.-F., Calvo, N., & Polvani, L. M. (2013). Climate Change from 1850 to 2005 Simulated in CESM1(WACCM). *Journal of Climate*, 26(19), 7372–7391. https://doi.org/10.1175/JCLI-D-12-00558.1

Marsh, P. T., Brooks, H. E., & Karoly, D. J. (2007). Assessment of the severe weather environment in North America simulated by a global climate model. *Atmospheric Science Letters*, 8(4), 100–106. https://doi.org/10.1002/asl.159

Meehl, G. A., Senior, C. A., Eyring, V., Flato, G., Lamarque, J.-F., Stouffer, R. J., et al. (2020). Context for interpreting equilibrium climate sensitivity and transient climate response from the CMIP6 Earth system models. *Science Advances*, 6(26), eaba1981. https://doi.org/10.1126/sciadv.aba1981

Mills, M. J., Richter, J. H., Tilmes, S., Kravitz, B., MacMartin, D. G., Glanville, A. A., et al. (2017). Radiative and Chemical Response to Interactive Stratospheric Sulfate Aerosols in Fully Coupled CESM1(WACCM). *Journal of Geophysical Research: Atmospheres*, 122(23), 13,061-13,078. https://doi.org/10.1002/2017JD027006

Moore, J. C., Yue, C., Zhao, L., Guo, X., Watanabe, S., & Ji, D. (2019). Greenland Ice Sheet Response to Stratospheric Aerosol Injection Geoengineering. *Earth's Future*, 7(12), 1451–1463. https://doi.org/10.1029/2019EF001393

Mukherjee, S., Mishra, A., & Trenberth, K. E. (2018). Climate Change and Drought: a Perspective on Drought Indices. *Current Climate Change Reports*, 4(2), 145–163.

https://doi.org/10.1007/s40641-018-0098-x

NASEM. (2021). Reflecting Sunlight: Recommendations for Solar Geoengineering Research and Research Governance. Washington, D.C.: National Academies Press. https://doi.org/10.17226/25762

NCEI, A. B. (2020). *U.S. Billion-dollar Weather and Climate Disasters, 1980 - present* (NCEI Accession 0209268) [Data set]. NOAA National Centers for Environmental Information. https://doi.org/10.25921/STKW-7W73

O'Neill, B. C., Kriegler, E., Ebi, K. L., Kemp-Benedict, E., Riahi, K., Rothman, D. S., et al. (2017). The roads ahead: Narratives for shared socioeconomic pathways describing world futures in the 21st century. *Global Environmental Change*, 42, 169–180. https://doi.org/10.1016/j.gloenvcha.2015.01.004

Orbe, C., Roekel, L. V., Adames, Á. F., Dezfuli, A., Fasullo, J., Gleckler, P. J., et al. (2020). Representation of Modes of Variability in Six U.S. Climate Models. *Journal of Climate*, 33(17), 7591–7617. https://doi.org/10.1175/JCLI-D-19-0956.1

O'Reilly, C. H., Befort, D. J., Weisheimer, A., Woollings, T., Ballinger, A., & Hegerl, G. (2021). Projections of northern hemisphere extratropical climate underestimate internal variability and associated uncertainty. *Communications Earth & Environment*, 2(1), 1–9. https://doi.org/10.1038/s43247-021-00268-7

Peters, G. P., Marland, G., Le Quéré, C., Boden, T., Canadell, J. G., & Raupach, M. R. (2012). Rapid growth in CO2 emissions after the 2008–2009 global financial crisis. *Nature Climate Change*, 2(1), 2–4. https://doi.org/10.1038/nclimate1332

Qin, J., & Robinson, W. A. (1993). On the Rossby Wave Source and the Steady Linear Response to Tropical Forcing. *Journal of the Atmospheric Sciences*, 50(12), 1819–1823. https://doi.org/10.1175/1520-0469(1993)050¡1819:OTRWSA¿2.0.CO;2

Rasch, P. J., Crutzen, P. J., & Coleman, D. B. (2008). Exploring the geoengineering of climate using stratospheric sulfate aerosols: The role of particle size. *Geophysical Research Letters*, 35(2). https://doi.org/10.1029/2007GL032179

Rasmussen, E. N., & Blanchard, D. O. (1998). A Baseline Climatology of Sounding-Derived Supercell andTornado Forecast Parameters. *Weather and Forecasting*, 13(4), 1148–1164. https://doi.org/10.1175/1520-0434(1998)013¡1148:ABCOSD¿2.0.CO;2

Rasmussen, K. L., Prein, A. F., Rasmussen, R. M., Ikeda, K., & Liu, C. (2020). Changes in the convective population and thermodynamic environments in convection-permitting regional climate simulations over the United States. *Climate Dynamics*, 55(1), 383–408. https://doi.org/10.1007/s00382-017-4000-7

Riahi, K., van Vuuren, D. P., Kriegler, E., Edmonds, J., O'Neill, B. C., Fujimori, S., et al. (2017). The Shared Socioeconomic Pathways and their energy, land use, and greenhouse gas emissions implications: An overview. *Global Environmental Change*, 42, 153–168. https://doi.org/10.1016/j.gloenvcha.2016.05.009

Richter, J., Visioni, D., MacMartin, D., Bailey, D., Rosenbloom, N., Lee, W., et al. (2022). Assessing Responses and Impacts of Solar climate intervention on the Earth system with stratospheric aerosol injection (ARISE-SAI) (preprint). *Climate and Earth system modeling*. https://doi.org/10.5194/egusphere-2022-125

Rodgers, K. B., Lee, S.-S., Rosenbloom, N., Timmermann, A., Danabasoglu, G., Deser, C., et al. (2021). Ubiquity of human-induced changes in climate variability. *Earth System Dynamics*, 12(4), 1393–1411. https://doi.org/10.5194/esd-12-1393-2021

Sardeshmukh, P. D., & Hoskins, B. J. (1988). The Generation of Global Rotational Flow by Steady Idealized Tropical Divergence. *Journal of the Atmospheric Sciences*, 45(7), 1228–1251. https://doi.org/10.1175/1520-0469(1988)045¡1228:TGOGRF¿2.0.CO;2

Schwarzwald, K., & Lenssen, N. (2022). The importance of internal climate variability in climate impact projections. *Proceedings of the National Academy of Sciences*, 119(42), e2208095119. https://doi.org/10.1073/pnas.2208095119

Seeley, J. T., & Romps, D. M. (2015). The Effect of Global Warming on Severe Thunderstorms in the United States. *Journal of Climate*, 28(6), 2443–2458. https://doi.org/10.1175/JCLI-D-14-00382.1

Sellar, A. A., Jones, C. G., Mulcahy, J. P., Tang, Y., Yool, A., Wiltshire, A., et al. (2019). UKESM1: Description and Evaluation of the U.K. Earth System Model. *Journal of Advances in Modeling Earth Systems*, 11(12), 4513–4558. https://doi.org/10.1029/2019MS001739

Simpson, I. R., Tilmes, S., Richter, J. H., Kravitz, B., MacMartin, D. G., Mills, M. J., et al. (2019). The Regional Hydroclimate Response to Stratospheric Sulfate Geoengineering and the Role of Stratospheric Heating. *Journal of Geophysical Research: Atmospheres*, 124(23), 12587–12616. https://doi.org/10.1029/2019JD031093

Simpson, I. R., Bacmeister, J., Neale, R. B., Hannay, C., Gettelman, A., Garcia, R. R., et al. (2020). An Evaluation of the Large-Scale Atmospheric Circulation and Its Variability in CESM2 and Other CMIP Models. *Journal of Geophysical Research: Atmospheres*, 125(13), e2020JD032835. https://doi.org/10.1029/2020JD032835

Smith, W., & Wagner, G. (2018). Stratospheric aerosol injection tactics and costs in the first 15 years of deployment. *Environmental Research Letters*, 13(12), 124001. https://doi.org/10.1088/1748-9326/aae98d

Stroeve, J. C., Kattsov, V., Barrett, A., Serreze, M., Pavlova, T., Holland, M., & Meier, W. N. (2012). Trends in Arctic sea ice extent from CMIP5, CMIP3 and observations. *Geophysical Research Letters*, 39(16). https://doi.org/10.1029/2012GL052676

Strzepek, K., Yohe, G., Neumann, J., & Boehlert, B. (2010). Characterizing changes in drought risk for the United States from climate change. *Environmental Research Letters*, 5(4), 044012. https://doi.org/10.1088/1748-9326/5/4/044012

Taszarek, M., Allen, J. T., Groenemeijer, P., Edwards, R., Brooks, H. E., Chmielewski, V., & Enno, S.-E. (2020). Severe Convective Storms across Europe and the United States. Part I: Climatology of Lightning, Large Hail, Severe Wind, and Tornadoes. *Journal of Climate*, 33(23), 10239–10261. https://doi.org/10.1175/JCLI-D-20-0345.1

Thompson, D. B., & Roundy, P. E. (2013). The Relationship between the Madden–Julian Oscillation and U.S. Violent Tornado Outbreaks in the Spring. *Monthly Weather Review*,

141(6), 2087–2095. https://doi.org/10.1175/MWR-D-12-00173.1

Tilmes, S., Richter, J. H., Kravitz, B., MacMartin, D. G., Mills, M. J., Simpson, I. R., et al. (2018). CESM1(WACCM) Stratospheric Aerosol Geoengineering Large Ensemble Project. *Bulletin of the American Meteorological Society*, 99(11), 2361–2371. https://doi.org/10.1175/BAMS-D-17-0267.1

Tippett, M. K., Allen, J. T., Gensini, V. A., & Brooks, H. E. (2015). Climate and Hazardous Convective Weather. *Current Climate Change Reports*, 1(2), 60–73. https://doi.org/10.1007/s40641-015-0006-6

Tippett, M. K., Lepore, C., & L'Heureux, M. L. (2022). Predictability of a tornado environment index from El Niño–Southern Oscillation (ENSO) and the Arctic Oscillation. *Weather and Climate Dynamics*, 3(3), 1063–1075. https://doi.org/10.5194/wcd-3-1063-2022

Trapp, R. J., Diffenbaugh, N. S., Brooks, H. E., Baldwin, M. E., Robinson, E. D., & Pal, J. S. (2007). Changes in severe thunderstorm environment frequency during the 21st century caused by anthropogenically enhanced global radiative forcing. *Proceedings of the National Academy of Sciences*, 104(50), 19719–19723. https://doi.org/10.1073/pnas.0705494104

Trapp, R. J., Diffenbaugh, N. S., & Gluhovsky, A. (2009). Transient response of severe thunderstorm forcing to elevated greenhouse gas concentrations. *Geophysical Research Letters*, 36(1). https://doi.org/10.1029/2008GL036203

Trapp, R. J., Hoogewind, K. A., & Lasher-Trapp, S. (2019). Future Changes in Hail Occurrence in the United States Determined through Convection-Permitting Dynamical Downscaling. *Journal of Climate*, 32(17), 5493–5509. https://doi.org/10.1175/JCLI-D-18-0740.1

UNEP. (2022). *Emissions Gap Report 2022: The Closing Window - Climate Crisis Calls for Rapid Transformation of Societies*. Retrieved from https://wedocs.unep.org/xmlui/handle/20.500.11822/40874

US Department of Commerce, N. (n.d.). *Severe Weather Definitions*. Retrieved April 4, 2023, from https://www.weather.gov/bgm/severedefinitions

van Vuuren, D. P., Edmonds, J., Kainuma, M., Riahi, K., Thomson, A., Hibbard, K., et al. (2011). The representative concentration pathways: an overview. *Climatic Change*, 109(1), 5. https://doi.org/10.1007/s10584-011-0148-z

Visioni, D., MacMartin, D. G., Kravitz, B., Boucher, O., Jones, A., Lurton, T., et al. (2021). Identifying the sources of uncertainty in climate model simulations of solar radiation modification with the G6sulfur and G6solar Geoengineering Model Intercomparison Project (GeoMIP) simulations. *Atmospheric Chemistry and Physics*, 21(13), 10039–10063. https://doi.org/10.5194/acp-21-10039-2021

Visioni, D., Bednarz, E. M., Lee, W. R., Kravitz, B., Jones, A., Haywood, J. M., & MacMartin, D. G. (2023). Climate response to off-equatorial stratospheric sulfur injections in three Earth system models – Part 1: Experimental protocols and surface changes. *Atmospheric Chemistry and Physics*, 23(1), 663–685. https://doi.org/10.5194/acp-23-663-2023

Wang, M., & Overland, J. E. (2012). A sea ice free summer Arctic within 30 years: An update from CMIP5 models. *Geophysical Research Letters*, 39(18). https://doi.org/10.1029/2012GL052868

Wei, H.-H., Subramanian, A. C., Karnauskas, K. B., DeMott, C. A., Mazloff, M. R., & Balmaseda, M. A. (2021). Tropical Pacific Air-Sea Interaction Processes and Biases in CESM2 and Their Relation to El Niño Development. *Journal of Geophysical Research: Oceans*, 126(6), e2020JC016967. https://doi.org/10.1029/2020JC016967

Weisman, M. L., & Klemp, J. B. (1982). The Dependence of Numerically Simulated Convective Storms on Vertical Wind Shear and Buoyancy. *Monthly Weather Review*, 110(6), 504–520. https://doi.org/10.1175/1520-0493(1982)110¡0504:TDONSC¿2.0.CO;2

Wilks, D. S. (2016). "The Stippling Shows Statistically Significant Grid Points": How Research Results are Routinely Overstated and Overinterpreted, and What to Do about It. *Bulletin of the American Meteorological Society*, 97(12), 2263–2273. https://doi.org/10.1175/BAMS-D-15-00267.1

Zarnetske, P. L., Gurevitch, J., Franklin, J., Groffman, P. M., Harrison, C. S., Hellmann, J. J., et al.

(2021). Potential ecological impacts of climate intervention by reflecting sunlight to cool Earth. *Proceedings of the National Academy of Sciences*, 118(15), e1921854118. https://doi.org/10.1073/pnas.1921854118